Design and Development of a LIVE Digital Twin Methodology for Predictive Maintenance of Bearings in Rotary Machine Systems

by

Tristan J.A. Zonta

A thesis submitted to the
School of Graduate and Postdoctoral Studies in partial
fulfillment of the requirements for the degree of

Master of Applied Science in Mechanical Engineering

Department of Mechanical and Manufacturing Engineering

Faculty of Engineering and Applied Science

University of Ontario Institute of Technology (Ontario Tech University)

Oshawa, Ontario, Canada

December, 2025

THESIS EXAMINATION INFORMATION

Submitted by: **Tristan Zonta**

Master of Applied Science in Mechanical Engineering

Thesis title: Design and Development of a LIVE Digital Twin Methodology for Predictive Maintenance in Rotary Machinery Systems

An oral defense of this thesis took place on November 28th, 2025, in front of the following examining committee:

Examining Committee:

Chair of Examining Committee	Dr. Martin Agelin-Chaab
Research Supervisor	Dr. Ahamad Barari
Examining Committee Member	Dr. Amirkianoosh Kiani
Examining Committee Member	Dr. Ebrahim Esmailzadeh
Thesis Examiner	Dr. Shabnam Pejhan

The above committee determined that the thesis is acceptable in form and content and that a satisfactory knowledge of the field covered by the thesis was demonstrated by the candidate during an oral examination. A signed copy of the Certificate of Approval is available from the School of Graduate and Postdoctoral Studies.

ABSTRACT

Digital Twin (DT) is a prominent focus for many predictive and prescriptive maintenance strategies. In maintenance, DT is used for connecting the physical and digital models of a maintenance monitoring system and proactively prescribing maintenance solutions to extend the products life. Many of the failures in modern DT can be attributed to the lack of defined structure, the unavailability of failure data to calibrate the systems, and poor connectivity between the physical and digital systems. LIVE provides a systematic approach to implement a DT system in 4 stages of Learn, Identify, Verify and Extend. This thesis uses LIVE DT for dynamic rotary systems connecting the physical asset to its DT to predict failure. In addition, this thesis covers the development of a device that will allow for emulating bearing defects in a controllable and repeatable way for calibrating virtual systems when historical or failure data is unavailable.

Keywords: LIVE Digital Twin; Smart & Predictive Maintenance; Data Analytics; Bearing Failure Data, Calibration of Digital Twins.

AUTHOR'S DECLARATION

I hereby declare that this thesis consists of original work of which I have authored. This is a true copy of the thesis, including any required final revisions, as accepted by my examiners.

I authorize the University of Ontario Institute of Technology (Ontario Tech University) to lend this thesis to other institutions or individuals for the purpose of scholarly research. I further authorize University of Ontario Institute of Technology (Ontario Tech University) to reproduce this thesis by photocopying or by other means, in total or in part, at the request of other institutions or individuals for the purpose of scholarly research. I understand that my thesis will be made electronically available to the public.

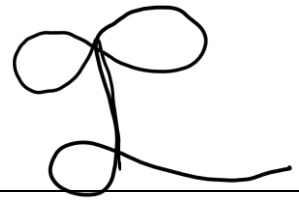

Tristan J. A. Zonta

STATEMENT OF CONTRIBUTIONS

The following research have been works I have contributed into during my time completing this work. Currently the works remain unsubmitted but are under consideration for publication in the future. In this research I have contributed to the design, building, and testing of the rotary system that is used in this thesis, in addition to working on the resulting Low-Fidelity and High-Fidelity simulation results.

Andrew Bondoc, Tristan Zonta, and Ahmad Barari, “The Calibration of a Scaled Prototype For Model Validation In a Live Digital Twin of Pipeline Systems,” p. 6, 2026.

Andrew Bondoc, Tristan Zonta, and Ahmad Barari, “Calibration and Validation of High and Low Fidelity Simulations for Health Monitoring LIVE Digital Twin of Bearings,” in *Verification, Validation, and Uncertainty Quantification Symposium*, Nashville, TN, 2026.

ACKNOWLEDGEMENTS

I would like to thank a great many people for their support over this long period of time in completing my graduate thesis.

I would like to especially thank Dr. Barari who pushed me to continue and work through the struggles when I wanted to quit many times throughout the process. I also want to thank Dr. Barari for the support and knowledge that he brings to our lab. I do not know if I would be able to finish this work without all the expertise he shared. He always makes time for the students and their research and ensures that we achieve our goals.

I would like to thank Mohsen Tayefeh for all his in depth knowledge and help through this thesis, he greatly helped with the development of my learning and his help cannot be understated. In addition, my fellow students of AD2M labs helped in many ways not only just academically but also socially when I am not have been in the best of spirits. They especially helped in giving lots of feedback during this time while still sparing some time for a few chess breaks, in addition to always bringing food to share with everyone.

I want to thank my friends who I was able to talk to through this time when I was down and needed support. I will never forget our gaming sessions, late night talks, and therapy sessions. These things meant a lot to me and will be great memories of this time.

Finally, I would like to thank my family, who were always the most supportive and understanding during this time. Never judge me for being busy and missing events, always being supportive in any decision I make and trust that I will do my best and succeed. All your efforts in helping me move, bringing me food, listening to me when I was down, and helping me when I inevitably ran into car trouble. I will forever be appreciative and grateful for all that you have done even if sometimes I don’t show it properly.

Thank you everyone for helping me strive to accomplish more than I thought I could.

TABLE OF CONTENTS

LIST OF TABLES

LIST OF FIGURES

LIST OF ABBREVIATIONS AND SYMBOLS

2PM	Prognostics and Predictive Maintenance
AD2M Labs	Advance Digital Design, Manufacturing, and Metrology Laboratories
AI	Artificial Intelligence
ANN	Artificial Neural Networks
BDI	Bearing Defect Inducer
BW	Backwards
CAD	Computer Aided Design
CAE	Computer Aided Engineering
CAM	Computer Aided Manufacturing
CE	Conformite Europeenne
CSA	Canadian Standard Association
DMLS	Direct Metal Laser Sintering
DOF	Degree of Freedom
DT	Digital Twin
FFT	Fast Fourier Transform
FW	Forward
HF	High Fidelity
IoT	Internet of Things
LIVE	Learn, Identify, Verify, Extend

LF	Low Fidelity
ML	Machine Learning
PdM	Predictive Maintenance
PLA	Polylactic Acid
PWM	Pulse Width Modulation
RM	Rotary Machines
RMSE	Root Mean Square Error
RPM	Revolutions Per Minute
RUL	Remaining Useful Life
SSB	Simple Structural Beam
UL	UL Solutions Certification
VFD	Variable Frequency Drive

Chapter 1. Introduction

1.1 Motivations and Problem Statement

The traditional maintenance system results in a lot of waste and impact on the environment, this is due to parts that experience failure earlier in their life span. It is beneficial to have a more intelligent system that can prescribe maintenance.

In the industry of manufacturing, maintenance strategies are essential to run a facility with minimal downtime and waste. Traditional methods may use reliability statistics or physical model-based approaches for fault prediction but can fall short due to their generalization. These methods face challenges in implementation; this can be for complex mechanisms and parts that are unique to a facility or for situations where there are many items and they all react differently. Historical data is extremely important for reliability statistics and testing, while physical model-based techniques depend heavily on the expertise of individuals in establishing accurate mathematical models. This can often lead to inaccurate predictions overlooking the dynamic nature of equipment over its lifecycle.

Following the fourth Industrial revolution, Digital Twin (DT) is considered a leading technology in smart maintenance and predictive maintenance (PdM) of physical systems. The ability to predict the onset of failure is critical when minimizing system downtime and monetary losses. A DT is defined as the bidirectional communication between a physical system and its virtual model. However, establishing these bidirectional connections is only advantageous through robust sensor technology and data analytics.

Rotating Machineries (RM) are used in many applications such as generators, pumps, fans, induction motors, tools and so on. It is highly desired to help various Canadian industrial sectors including sustainable energy and transportation's infrastructure to improve their asset management with focus on appropriate maintenance on heavy duty and critical RM. These important assets are widely used in extremely critical infrastructure and can be vulnerable to failure in use.

The need for this development was well realized during the recent unfortunate pandemic. Due to the pandemic, the presence of the maintenance crew in such facilities was

significantly decreased. Regular in-person inspection of the critical RM in hydropower, wind energy, and transportation facilities was interrupted. Rotating Machineries typically deteriorate their balance condition dynamically, due to wear, thermal bending, process dirt collection, etc., and gradually develop concerning vibratory unbalance responses which result in machine failure. From the electrical point of view, insulation failure, deformation of stator/rotor bars, experiencing partial discharge, experiencing fault currents, and thermal stress due to overcurrent or overloading would also affect RM performance and lifespan. Significant costs of repairs can be attributed to the failure of rotating machinery in applications ranging from electromotors and generators to wind turbines or pumps, in extreme cases this may put human life in danger. Governments and industries put a great deal of resources into the study of rotor dynamics to calculate the 'safe' operating ranges before the machine goes into service and methods of detecting imminent failure.

The methodology of using LIVE DT for prognostics and predictive maintenance presented in this thesis is innovative and novel. Traditionally, prognostics and diagnostics are done manually and during times of outage inspections in the target highly critical infrastructures. LIVE DT allows for real time visualization of the current health of RM assets without interrupting their operation and can provide insights into how current modes of operation affect expected equipment longevity.

Considering the novelty of LIVE DT and its application in prognostic and predictive maintenance, research and development in this area places Canadian industries in an international leading position internationally. The developed technology can be exported to many Canadian companies and industrial sectors internationally, energizing the Canadian economy. The research team at AD2MLabs is highly capable in developing High Fidelity and Low Fidelity multi-physics simulation, digitalization, inspection and metrology, sensor design, digitalization in design and inspection, and CAD/CAM/CAE.

1.2 Approach and Research Objectives

In this thesis the core objectives that are aimed at being achieved is to address many of the issues that are seen in existing implementations of DT systems in literature. LIVE DT is the methodology implemented to achieve these goals. LIVE DT has been implemented in

many case studies and lab environments but never for a dynamic system such as rotary machines. This is a core objective pushed by industry partners to show the implementation of LIVE DT on a dynamic system rather than a static system which is to be completed in this thesis.

In addition, the DT must be able to produce a reliable and repeatable way to generate failure data for pre-defined damage levels on the physical entity. Running the machine in its normal operating condition will take too long to experience failure conditions and thus alternative approach must be taken. The failure data must include the known damage and data of failure. The failure data from the bearing defect inducer (BDI) is used to bridge this gap in creating failure data with predefined failure amounts. This system is then used to calibrate the high-fidelity model. Due to the cost of high-fidelity limited samples need to be used to be able to calibrate with low level of fidelity. This is the second objective of this thesis to develop the BDI in a repeatable and efficient way to generate failure data that others can repeat for their own bearing rotary systems.

Finally, the last core objective is the use of LIVE DT establishing the connection between the virtual and the physical. LIVE DT demands for integration and communication among 3 entities in comparison to the typical 2 entity system found in traditional DT systems. These 3 entities consist of the physical machine, High-Fidelity (HF) simulations and Low-Fidelity (LF) simulations. HF consists of using high detail multi-physics simulations to understand the nature of the system. LF can be based on a data driven method, a lower complexity version of the HF but with similar physics or can be a combination of the 2 methods incorporating both data driven and reduced complexity models. Therefore, the first objective is the implementation of LIVE DT to connect and calibrate the physical system with the virtual LF and HF models. The calibration between the 3 entities creating LIVE Triplets capable and thus reaching the same output conclusions on system health is the final goal. When the triplets receive the same input they should produce the same output, eventually being able to predict the health of the system and give advice as to when maintenance should be performed. Thus, the final core objective is this calibration between the 3 entities able to produce the health of the system and recommended action by the user.

1.3 Thesis Outline

The following thesis will be presented over a course of 5 chapters. The first chapter provides the background of the problem being studies and the objectives of the work being completed. Chapter 2 will look to give a descriptive theoretical background in topics such as DT, smart maintenance and condition monitoring in industrial and test settings. Additionally, it will also investigate details on bearings and the LIVE DT process. Furthermore, chapter 3 will look to discuss the methodology and design of the test rig, the design and implementation of a failure generating device known as the BDI, as well as how they both fit into the methodology of LIVE DT, and a discussion on Low-Fidelity and High-Fidelity Models. Chapter 4 focuses on the calibration of the LF and HF models and the results of the design and failure data it creates in collaboration with the complete multi-physics simulation results. Then the final chapter 5 will focus on conclusion and future works.

Chapter 2. Theoretical Background

2.1 Digital Twins

DT is a technology with the potential to improve the quality control of any physical system and is constantly seeing innovation and improvements. There are many methodologies of DT such as Prognostics and Diagnostics, PdM and other are essential health management tools. DT is the idea of having a physical system and a virtual counterpart that communicate between each other to have better monitoring results. DT proves to have superior capabilities in prognosis and diagnosis when compared to traditional practices such as time-based maintenance or condition based [1], [2]. A DT can be implemented on various levels from focusing on just a singular component or on a system or systems of systems level [3]. A example of component level item may be a bearing, a system level a rotary machine attached to a shaft, bearings and other components, and finally a system of system can be a collection of these motor systems in an entire industry plant [4].

Maintaining real-time communication between the physical and digital is a difficult task. The calibration process is an important part of DT systems. Sensor data must be properly transferred while noting the risk of noise, latency, or data mismatch to ensure calibration is successful [4], [5]. One of the more common ways of measuring data for DT is using vibration data. Vibration is a useful way of measuring data due to its presence in all machinery experiencing dynamic loads such as motors. This data is valuable in understanding the effects of resonance, fatigue, and other general system failures [6]. A common technique of Modal Analysis is used when capturing the health of any physical system or component such as fluid conveying pipelines [7], buildings [8], and any other physical system [9].

An important part of a DT system is its sensor network. This network should prioritize minimizing the quantity of sensors while maximizing the probability of damage detection [3], [10]. An optimized sensor network can be further supported with effective simulations provide a more comprehensive understanding of the physical system [11]. Inversely, sensor setups that are not sufficient can reduce the system's sensitivity to fault conditions and exponentially increase the amount of transmitted data [12]. This makes the filtering process

an important step in health monitoring. Methods such as Fast Fourier Transform (FFT), time domain and frequency domain statistics, and wavelet transforms all contribute to the success in prognostics and diagnostics [13]. Transfering the data into the frequency domain allows for more accurate health predictions. This is also validated by Bondoc et al. (2024) on a lab scale prototype of a pipeline system [14]. Methods to detect wear or fault in the system include increases in vibration amplitude, and narrow band region energy, amplitude offsets, sideband frequencies, and truncated waves [15]. In general, amplitudes are inversely proportional with increasing frequency. For vibration applications, acceleration, velocity, and displacement sensors are all typical methods to capture the output signal of a system [6].

In literature, there are three categories which define the DT digital domain: Model-based, data-driven, and a hybrid-approach [16], [17], [18]. Each of the mentioned approaches can produce an effective DT for PdM and are expanded below.

Model-based method: In the physical model-based approach, a mathematical model is created based on how the system works. This model can be used in a procedure to reflect the overtime decline in the system's performance, helping to predict faults accurately. While this method doesn't require extensive data collection, it does rely on experts to design and build the model. However, because many systems are complex, it's challenging to accurately establish degradation models without understanding how they degrade.

Data-driven method: In the data-driven predictive maintenance method, data is collected from the studied devices for use in evaluation. Some of the ways in which this data is analyzed include methods like autoregressive modeling, artificial neural networks, support vector machines, and Gauss regression. The historical data of the devices is transformed into system knowledge and then analyzed for information about the system's health and degradation. This information is gathered through many sensors installed on the system being studied. One of the major challenges of this method is the lack of sensors making data collection and analysis challenging. Additionally, different algorithms can result in different levels of accuracy requiring experimentation to find the most suitable algorithm and parameters.

Hybrid Approach: To address the shortcomings of the methods mentioned earlier, many researchers have suggested the hybrid predictive maintenance approach. This approach combines the strengths of model-based and data-driven methods by creating a fusion between them. However, implementing the hybrid predictive maintenance approach requires building accurate mathematical physical models, gathering reliable real-time operational data, and conducting effective data analysis. Currently, mostly used hybrid algorithms are Kalman filter, Particle filter, and ensemble learning [19], [20].

Kritzinger et al. (2018) provides an overview of the state of the art of DT [21]. Various engineering disciplines were addressed in their review, and they discuss the various integration levels of DT such as the digital model, digital shadow, and DT.

Digital Model: In a digital Model there is no interaction or data exchange between the digital and physical object. Thus, any change to the virtual model must be done manually. In this model the physical object may be represented digitally through mathematical models, or characteristics of the object itself. For example, a motor characteristic might be the Finite Element Method of a motor or the 3D CAD model of it.

Digital Shadow: A digital shadow is the next level up from the digital model. In this scenario there is automatic data transfer in one direction from physical object to the virtual object. This can come in the form of various sensors like current, temperature or vibration sensors. Therefore, if there is a change to the physical object the digital object would be able to replicate or shadow it using the live data it receives from the physical model but the digital model is unable to affect the physical model. The digital shadow is just replicating the output of the system visually showing the user what the current system information looks like.

Digital Twin: DT is the 3rd step where the data transfer is fully automatic both ways and both sides can take data from the other and use it. For example, the digital object may be able to control parts of the physical model. This allows each model to work together to create a full picture and provide the most accurate condition of the system. The communication going back to the DT can be in the form of recommendations for maintenance.

2.2 Digital Twin for Design

Industry 4.0 has led to many great improvements in the field of design, one of which is pertaining to DT. Tao et al. (2019) propose a framework to connect the physical artifacts and their digital counterpart in more than just fault diagnosis [22]. This framework aims for the development of DT systems by manufactures to use the information received from their DT to improve their designs of bicycles. The framework methodology presented works by building a virtual representation using Computer Aided Design (CAD) for 3D modeling of the product. Through these design data can be processed to make informed design decisions based on simulating the behaviors in real-time communication between the physical and digital models. From there physical adjustments based on virtual model and gathering lifecycle data from the physical to refine the design. This was demonstrated in a case study involving bicycle design resulting in reduced design time, and improved customer satisfaction.

In similar work of this framework, it explores how DT technology can be extended to encompass the full lifecycle of a product, including design, manufacturing, and service [23]. The propose 3 phases of conceptual design, detailed design, and virtual verification. Conceptual design defines the product concept, how it looks, its functions, in addition to similar sales data, and customer feedback. Detailed design takes DT input of performance and testing data to improve upon the design. Finally, virtual verification expedites the initial production phase by catching many of the errors that may be seen in quality and defects of initial product production through its simulations. Another proposed implementation of DT is modeling of the manufacturing floor in a virtual space allowing optimization of resources and processes to any real time changes. Lastly, product service phase works like most DT in that they take data from their products to improve their reliability through maintenance strategies. The authors acknowledge that the main challenge in this process is between physical and digital connection is the demanding and resource-intensive simulations and calibration that need to occur to ensure it works efficiently and as needed.

The integration of DTs into Internet of Things (IoT) environments is another significant DT application. Through the replication of these physical IoT devices in virtual environments it allows designers the ability to improve the efficiency and effectiveness of IoT systems [24]. This early-stage development in efficiency leads to greater reliability and scalability of these systems down the product road while being able to be tested and adequately monitored.

Another major consideration when it comes to DT deployment and design is sustainability [25]. The authors introduce an additive energy consumption model to quantify the environmental impact of DTs. The framework breaks energy usage into multiple categories consisting of design, execution, networking, processing, and lifecycle updates. It is stressed that the importance of reducing the ecological footprint of DTs while maintaining the required accuracy to accomplish its goals is essential for sustainability. This is an important subject that is still lacking in many areas and requires the creators of DT systems to be selective in their modelling for sustainability.

The backbone of DT systems are the benefits received from the simulations and analysis. When considering the software engineering involved in these systems they can amount to significant technical debt [26]. As DT solutions grow in complexity, their design can accumulate inconsistencies resulting in large amounts of costs. These can lead to issues in scalability and adaptability, especially in systems that cover a large amount of data or users. The authors discuss a model to help reduce technical debt through the management of DT architecture. The author suggests that a standardization of design can lead to reduced technical costs.

Another piece of literature discusses the design of DT for selecting DTs within a System-of-Systems approach [27]. Their framework looks to use performance indicators to identify the best DT method for each individual system. The goal of this process is to ensure that the DT selected provides the most accurate and relevant results. This process is achieved through iterative feedback loops to pick the most effective DT system.

DT for design is also applicable for business applications to simulate and optimize business workflows [28]. They explore how Petri Nets can be used to model real-time business states. Their focus is on how real-time data and ML can be used to make business more efficient and flexible. Due to the lack of sensor data, the results heavily rely on the ML and analytics to function and not fully encompassing the real-time components of DT.

2.3 Digital Twin for Maintenance, Prognosis, and Remaining Useful Life (RUL)

When considering maintenance strategies statistical and physical model-based approaches have been the common approach for fault prediction. The problem these methods face in their implementation is due to the large costs associated with creating and maintaining these systems. This is especially true for complex and costly equipment such as nuclear power plants or industries with a lot of mechanical components like a car manufacture. Reliability statistics require large amounts of historical data and testing, while physical model-based techniques depend heavily on the expertise of individuals in establishing accurate mathematical models. Without the proper amount of data or expertise many of the dynamics of equipment or system can be overlooked during its life leading to inaccurate predictions.

In industry 4.0, the technological advancements in the ways of sensing, monitoring, simulation, and artificial intelligence have revolutionized maintenance strategies. Using these advancements, it makes the use of DT as a suitable approach offering real-time monitoring leading to future predictions on the condition of physical entity. DT serves as a platform for both models and data, enabling the representation of physical objects in virtual space, thereby facilitating the connection between the physical and digital [29].

When it comes to DT one of the primary uses for it is in the world of maintenance. DT is a useful tool that can save companies significant downtime and money by optimizing the maintenance schedule. Within maintenance there are a few different levels The levels are as followed.

Reactive: In this strategy maintenance is done as it is needed. A component will be run until failure and then it will be changed. This strategy is not very effective as it is unknown when an item will break and may cause unexpected downtime and large costs.

Preventative: When it comes to preventative it is the next step forward where a component will have a set time in which it can operate before it is changed prematurely to avoid unexpected downtime. This causes waste in changing parts well before their useful life is up.

Condition Based: This strategy entails watching some sort of indicator for example a vibration sensor. Once the vibration sensor reaches a predetermined vibration level this signifies it is time to change the part. This is more effective than preventative but does not inform what cause the fault and does not provide any remedies.

Predictive: For predictive this could use some form of simulation be it model or data based to predict when an object will fail based on data. This can be useful to know exactly when the best time to change is.

Prescriptive: Lastly, prescriptive takes predictive to the next level where it not only predicts when it is going to fail it can also determine what is going to fail and what the best course of action can be taken to reduce, mitigate, or extend the life of the object.

The objective of Vathoopan et al (2018) is to provide a methodology for modular corrective maintenance DT to assist human technicians identify and fix and faults found within an automated system [30]. The methodology in this article is to use existing data already collected previously along with premade elements within the OpenModelica software to create the corrective maintenance simulation layout. This is designed this way to specifically target individual faults or monitor an ideal model. The results of this research are very early in their implementation of corrective maintenance approach.

Tao et al. (2018) focuses on creating a method of approach to DT for complex systems that focuses on Prognostics and health management by providing a case study on a wind turbine system [28]. This article relates to other literature as it is another example of an outline on creating a DT while providing an example of a system it can recreate. The approach used in this article is stated to be a five-dimension DT which differs from a previous 3-dimensional DT that only considered the virtual model, physical model and connections. This 5 dimensional has additional dimensions for DT data and services which combine data from digital and physical to predict faults and provide proper instructions on

countermeasures. Similar to other research, the implementation is only in the form of concepts with some datasets provided with no real testing on physical models.

Two less addressed challenges in developing data-driven fault diagnosis methods are insufficient training data specifying diagnosis information. Xu et al.(2019) addresses these two concern through generating synthetic data and then using Deep Transfer Learning to deal with data in different forms with related contents [31]. A high-fidelity virtual model is then generated to anticipate potential failures under different parameters.

Similarly, Werner et al. (2019) recommends a hybrid approach that combines the data driven of data collection to make predictions using statistical methods. Physics based modeling uses created models and theoretical values for the inputs. This means getting real time data to help predict future changes and estimate remaining useful life. Useful tools for data drive approaches may use a variety machine learning algorithms such as classification and regression or clustering for data analysis. Physics based modeling uses reliability methods such as failure mode and effects analysis.

Aivaliotis et al. (2019) aimed to create a basic outline that can be used to create a DT for various predictive maintenance applications using physics-based modeling [32]. This article is relevant to the literature as there is no standard outline on how to produce a DT in the industry. The authors look to create a concept to fill that lack in research in a way that is still applicable to many fields of maintenance. The methodology used was split into 3 phases, the first phase is to model the machine in which is being studied, the second phase was to model the virtual sensors, and the third was to define the variables that need to be changed in the model in order to reach a similar state as the model it looks to imitate. Implementation of this method was strictly virtual and conceptual and not a full implementation, so it fails to fully explore this topic.

Aivaliotis et al. (2019) expands on the previous work by using physics-based models to generate DT of machinery components with the goal of predicting their Remaining Useful Life [33]. Here, RUL calculation happens at a component-level, independent from the use of past failure data in hand. Turning a physics-based model into a DT happens through the calibration of their simulation mechanism, this will match the actual condition of the system with the digital representation of the machine in real-time. The procedure to reach

RUL passes through four stages as followed. The first phase involves advanced physical modeling of the machine using Physics-based modelling, starting with defining the kinematic and structural models. Calibration then adjusts the physics-based models to create the DT in the simulated environments. Furthermore, DT operation focuses on modeling and tuning machines in Phases 1 and 2, the next step involves simulating the tasks assigned to real machines. The virtual outcomes from this simulation, compared with the actual outputs of real machine operations, are used for calculating the RUL. Then by looking at the degradation model and the planned future operations and continuous simulations it is then possible to predict the RUL of the machine which is compared continuously with the normal machine output.

Ding et al. (2019) follows a hybrid approach to predict abnormality in shearer key parts and alarm to stop for inspection [34]. The hybrid approach consists of a qualitative part and a quantitative one. The qualitative part is done through model-based approach, and the quantitative part is working with data-driven method, and then the result from two are fused to decide on the final decision, whether the shearer should be stopped or not. In the next step, RUL prediction happens in two stages, data pre-processing and model prediction, it goes through different methods of evaluation to determine the best neural network method for RUL calculation.

In the context of rotating machinery, DTs serve as cyber-physical systems capable of supporting tasks such as vibration monitoring, fault diagnosis, and predictive maintenance. The virtual models replicate the dynamics of mechanical components such as shafts and bearing. This then allows them to be simulated, analyzed, and optimized for their system behavior without the physical intervention that may be needed for many sensors. The lab-scale prototype focussed on generalized components such as the electric motor due to its relevance in various industries [35]. This potential prototype is easily manufacturable in the confines of a university laboratory. However, it is also important to consider the potential faults and damages experienced by industry machines. Motor damages such as overloading, rotor failure, and contaminants were commonly experienced [36].

Various sensors can be used ranging from displacement, velocity, acceleration, and force sensors instruments. But most available industrial devices use vibration acceleration or

velocity sensors [37]. This is because rolling elements emit a wide spectrum of frequencies and will capture the absolute vibration of the bearing and the entire system it's mounted on.

Wang et al. (2018) produced a DT for rotating machinery for intelligent fault diagnosis [11]. Employing both digital simulations and empirical data, they perform time and frequency statistical analysis for enhanced PdM with a diagnosis error of less than 5%. Dos Santos et al. (2022) develop a DT of an electric motor for the purpose of PdM [38]. Using sensor data, they measure the temperature and current of the electric motor to diagnose the faults in the system and reduce the downtime. The data is fed to a finite element method magnetic software to validate the real-time data.

Goundar et al. (2015) developed a prediction model for electric motors using vibration and temperature sensor data [39]. Leveraging Internet of Things (IoT), they successfully monitor the condition of the motor based on their sensor locations. They discuss the importance of sensor placement in relation to the motor as various positions can be considered too invasive causing distortion in the data. The data from the accelerometer was also processed using FFT. Hu et al. (2023) produced a DT for the fault monitoring and detection of Induction Motors [40]. Using a frequency transform is an excellent method to reduce the strong noise interference typically experienced by high RPM motors. They employ a Bayesian data-driven methodology to extract potential faults in their motor output signal.

Several of the articles studied in literature review were separated into the 3 prior mentioned categories of condition based, diagnosis was, and prognosis in Table 2-1.

Table 2-1 Article Classification

		Goal					
Ref	**Year**	**Condition-based**	**Diagnosis**	**Prognosis**	**Maintenance Scheduling**	**Framework**	**Case Study**
[21]	2018					No	No
[30]	2018		✓			No	Yes
[41]	2018		✓	✓	✓	Yes	Yes
[42]	2019		✓	✓	✓	Yes	Yes
[31]	2019		✓			Yes	Yes
[43]	2019		✓	✓	✓	Yes	No
[44]	2019		✓	✓	✓	Yes	Yes
[33]	2019			✓		No	Yes
[34]	2019			✓		No	Yes
[45]	2019		✓			Yes	Yes
[32]	2019		✓	✓	✓	Yes	Yes
[46]	2019			✓		No	Yes
[47]	2019		✓	✓		Yes	Yes
[17]	2020			✓	✓	Yes	Yes
[48]	2020	✓	✓			Yes	Yes
[49]	2021			✓		Yes	Yes
[50]	2021		✓			Yes	Yes
[9]	2021		✓	✓	✓	Yes	Yes
[38]	2022		✓	✓		Yes	Yes
[51]	2022			✓		Yes	Yes

2.4 Digital Twin for Automation and Robotics

With respect to Industry 4.0 DTs look to combine the physical and the virtual with intelligent automation making use of IoT and AI. Pires et al. (2019) shows a case study by developing a DT of a collaborative robot using V-REP simulation software [52]. This example shows how DTs can simulate, monitor, and control physical operations in real-time, improving industrial automation capabilities. The authors study also focuses on some of the major issues of DT technology such as data standardization, real-time data feedback, and communication between system components.

Using web services to retrieve data from the DT and implementing an augmented reality system to visualize it are the two main components of the methodology described in the article in [53]. A DT product, simulation, and manufacturing data is made easily accessible through web browsers thanks to the proposed architecture. Utilizing the Unity Integrated Development Environment the augmented reality application is implemented. A case study is included in which an augmented reality system is utilized to visualize data that is retrieved via web services from a supervisory system that acts as a data repository. The case study demonstrates the effective use of web services to retrieve data in real-time from the DT and the augmented reality system's visualization of this data. It demonstrates that a cyber physical system is composed of an interactive visualization system for human interaction, a decision-making system, a data management system, and a data collection system from sensors. This architecture's objective is to use Augmented Reality systems to visualize physical data within the framework of a cyber-physical system.

Enhancing the collaboration between humans and industrial robots with an emphasis on improving safety measures is important for future progress in production. This objective was focused on by Droder et al. (2018) through the implementation of ML Artificial Neural Networks (ANN), to manipulate industrial robots [54]. The goal was to see how industrial robots could demonstrate improved path planning and obstacle avoidance through the application of ML methods while prioritizing the safety of the operator. The research was able to demonstrate proof of concept for adaptive path planning and object detection. One

of the stated problems of the research that was highlighted were the limitations in the reliability of recognition and processing speed.

As seen by Denk et al. (2022) DTs can be used to replicate entire environments which are useful for autonomous navigation [55]. The authors use a technique called homotopic shrinking to eliminate non-efficient paths in an unknown environment. The authors simulated their environment in MATLAB and did not have any physical implementation thus not fully implementing their DT and is only a case study.

Like most DT and maintenance problems, a major point of concern is the lack of failure data. Song et al. (2022) performed a study on the replication of the joints of a robot using DT and neural networks [56]. The goal of the investigation was to highlight faults that occur in the robot arm through use of the DT. A dynamic model is constructed and compared with physical robot arm degradation results and failure data was generated from this DT. It was seen that faults can be diagnosed and identified 32.5% more frequently through the simulated model using only 400 samples to create the generated data.

Autonomous vehicles are becoming the standard in many applications from consumer vehicles to delivery and even construction. Some examples of this include the use of DT such as Boros et al. (2023) and involves the design and analysis of an autonomous cone placing robot [57]. The authors detail their design methods and construction of both the physical robot and the DT. The main contribution of the work is that there are few physical prototypes for this cone-placing application. There is not much contribution to the methodology of DT, but it highlights the importance and communication between the robot its sensors and the robot operating system. Some additional examples of robots like this include Grazioso et al. (2023) that look to validate their designed multibody twin against the studied prototype. Furthermore the DT is used to monitor and record the robots ability in real time [58]. Xu et al. (2023) accomplishes similar goals in their article [59] but are able to incorporate human and robot together with DT to improve the stability of their trenching machine. It is capable of path planning, obstacle avoidances, mapping, and improvements on the standards needed to be met. Some additional robots that work outside

autonomously by applying DT applications include a snow blower robot [60] and patrol robot [61] and [62].

Some more niche examples of DT in robotics include disinfection robots made especially popular during the time of COVID-19. These robots use the power of UV light as a tool for disinfection and required the use of a DT in a virtual environment to be able to function [63], [64]. The DT virtual environment allows them to map the area, navigate it while avoiding obstacles and optimally path plan in the area. Similarly unique applications include thermal DTs researched by Aden et al (2023) in which they study the distribution of heat in buildings [65]. It continuously updates a 3D thermal model of the building for use in future energy analysis projects.

In the article by Wang et al. (2021) they investigate using UR5 robots equipped with DT in combination with people. The first article focuses on the application of welding robots common in many manufacturing assembly robots [66]. The human controls the robot through virtual reality and then the robot will then relay the welding scenes back to the users. A data driven approach is used with various techniques allowing for 94.44% classification accuracy recognizing skilled welding workers which can help the training of newer workers.

Overall, the use of DT in automation and robotics is very important to the future of improving these systems for safety, efficiency and health. It is used in many applications of autonomous vehicles capable of completing many different tasks. In addition, it is useful for robotics for manufacturing plants and other typical manipulator tasks that often take a lot of time to prepare or train for. Some of the major issues still exist in that it is difficult to implement an entire DT system and that many are only successful in completing portions of DT systems.

2.5 Human Digital Twin

COVID-19 was a significant event that affected many people's lives. Lv et al. (2021) designed a DT of an assembly line with the focus of analyzing the effects of COVID-19 in close quarters work spaces [67]. Both human components and robots are used in the study, however the study is conducted purely in simulation with future development including a physical trial. The author proposes a methodology of a deterministic policy gradient to optimize the productivity on the assembly line within the confines of new requirements put forth by COVID-19 restrictions. The results showed that the efficiency of tasks increased by 25.09% while the operator workload was reduced by 20.24%. The main issue with the article is the lack of HF digital model or physical implementation to confirm accuracy.

Another interesting work by Galarza et al. (2023) allows a person to perform teleoperation control over a robot with attached robotic arm and able to perceive what the robot sees with its camera in a constructed virtual reality [68]. The main contribution of the research is to develop a training environment for users to become efficient with the operation of robots. The final goal of this study is to make an impact in the areas of virtual social interaction for the elderly to allow for virtual reality motion for those who may be unable to walk or have other health issues. This is also explored in the article by Lee et al. (2022) where teleoperation is performed through the visual recording of different human poses to a real collaborative robot. Using the framework the author believes that industrial levels of speed can be achieved using their human DT framework. The teleoperation controls working in real time allow it to achieve these feats.

Continuing the heathy and well-being of people a study by He et al. (2021) involving an autonomous massage chair. The authors analyze the detection methods for pressure and force of the massage chair to build a DT that will match the force in a simulated environment [69]. A secondary section of the study involves training the DT with physical data to ensure a simulated human is not injured and then this data is fed back and used to control a physical massage device. The authors used data fusion to record the pressure levels on different body parts from the chair to develop an overall performance level of the massage chair. The authors aimed to optimize the massage chair components using the DT

model to see if material can be reduced to achieve the same pressure from a portion of the chair.

Chakshu et al. (2018) proposed the use of a DT model to detect the severity of carotid stenosis from a human face. The method is described as using coupled blood flow and a head vibration model, that is capable of linking a external videos of a patient's face without any contact, to carotid occlusion [70]. A head vibration model is proposed as the vibrations generated by blood flow can indicate carotid stenosis severity. Computer vision algorithm is implemented to use human face videos to determine the head vibrations which are compared with the vibration data. It can correctly predict the anticipated oscillations of the head vibrations. The one concern with this case study is the small sample size due to the nature of people getting treatment and thus required the creation of artificial stenosis patients.

Barricelli et al. (2020) they implemented a human DT that predicts the physical twin performance during fitness training and suggests modifications in their behavior [71]. SmartFit was the computational framework used that allows for monitoring team members' behaviors using wearable sensors. One limitation of SmartFit is that not all data collected can be continuously collected using Wi-Fi connected sensors and must be manually signed. SmartFit will be used in the future for collecting historical dataset from a professional team of athletes to develop more stable and complex models. As the training data becomes significantly larger the training process time increases. The author looks for future works to use incremental learning methods in order to efficiently use training data on limited computing resources without sacrificing accuracy.

In [72] they claim their emotion recognition based on body movement and facial expressions is a novel approach to human DT. They use three devices to construct a bi-modal database containing the six emotional states of seventeen participants. The acquired findings demonstrate the effectiveness of the combination of 3D distance and 3D angle in characterizing and identifying emotions. The body modality produced consistent results and the comparison revealed that the proposed methodology outperformed other forms of

classification accuracy. Future applications might involve emotion recognition and VR technology into the human DT.

Saul et al. (2024) aimed to create a system with the purpose of monitoring their workers mental, physical, and emotional states [73]. The goal of this approach was to enable the identification of emotional factors that may affect worker safety. Their idea is a theoretical one in nature that people give of signs in body language and emotion that will potentially lead to or are signs of negative health effects. Eventually, technologies like AI will lead to the development of safer work for multiple and create risk assessments for companies and their employees to ahead on their safety and improve their ability to perform safety interventions.

2.6 Conclusion on Digital Twin Literature

Overall, many of the works of literature present many methods for developing a DT. From these works successful DT structures look to pull information from various sources be it historical data, failure and test data, expert advice, mathematical models, etc. Therefore, taking a hybrid-based approach is one of the more successful methods for developing a DT system. In addition, from the various literature works it is evident that there are a few major concerns and best practices that span across the many DT presented. One of the common concerns is that many of the examples are only in a digital setting and are not applied in the physical world. This already makes them not a full digital twin but more of a digital model. The next concern is that many of the applications lack failure and historical data that can be used to complete the model and needs a solution. These are all items that look to be covered and addressed in both the LIVE DT methodology and the achievements of this thesis.

2.7 LIVE Digital Twin

The LIVE DT methodology is one that has been outlined in various literature to provide a standardized structure and framework for DTs. This methodology incorporates many of the advantages from the various other literature covering this topic. The proposed structure by Malek et al. (2021) is a four phase approach to developing DTs for PdM [9]. The structure is laid out by the acronym LIVE which represents the four phases to creating a

DT and stands for Learn, Identify, Verify, and Extend. This methodology, in continuous development for many years and has been detailed in multiple case studies published by AD2M. The applications in which this process has been applied includes railway systems, pipeline infrastructures, belt conveyor mechanisms, and rotary machinery [9], [12], [14], [74], [75], [76]. The complete methodology is visually represented in a DT platform framework composed of these phases as seen in Figure 2-1.

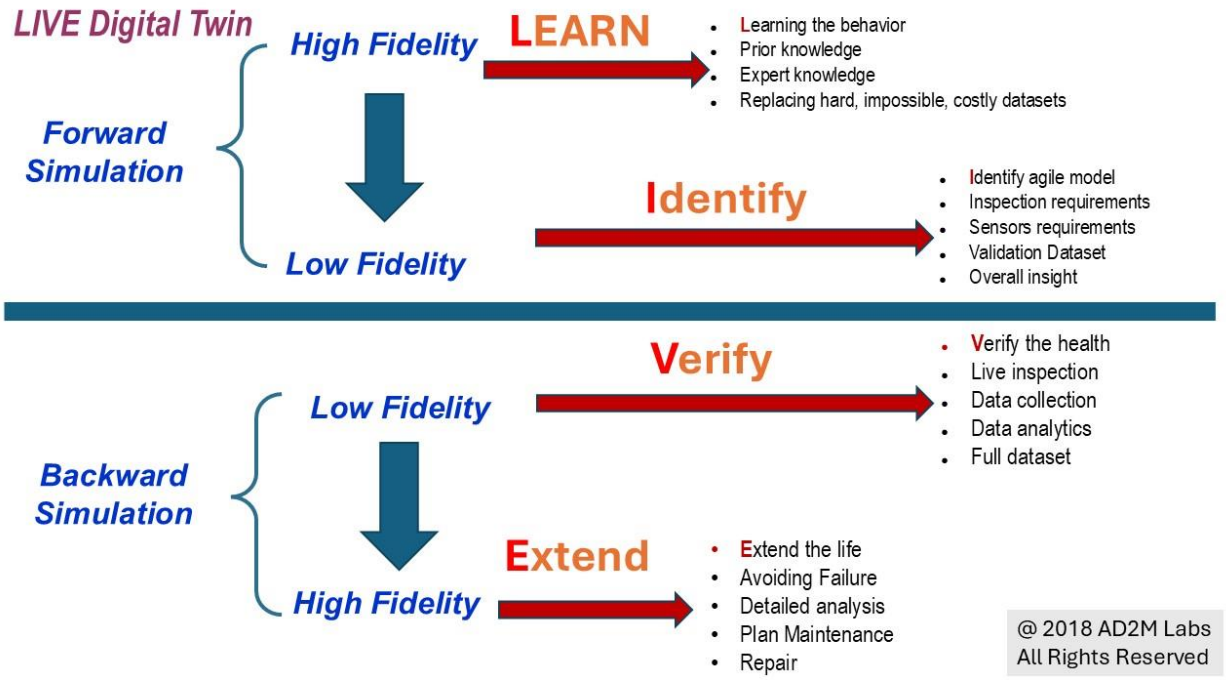

Figure 2-1: LIVE Digital Twin Architecture [9]

Taking a deeper look at the DT architecture in Figure 2-1 the methodology looks at two core simulation types, forward and backward each applied over 2 of the prior mentioned phases. In order to explain the difference between these 2 methods of simulation Bondoc [12] based on works from [8], [9] uses a fixed-free cantilever beam as an example.

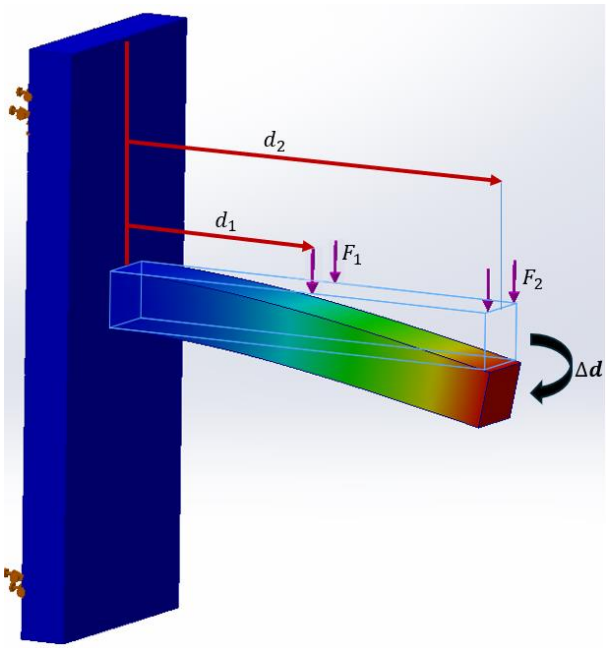

Figure 2-2: Fixed Free Cantilever Beam [12]

Continuing, in Figure 2-2 the fixed free cantilever beam is shown with 2 vertical force components labeled F_1 and F_2 at locations d_1 and d_2 respectively. These forces and distances cause the free end of the beam top displace by a displacement of delta. In solving a problem like this a certain number of known conditions are required and that determines the simulation. Forward simulation is based on a physics driven model defined by the external conditions on the beam. For example, if the amount of force applied at the defined points is known along with the locations that these forces occur then the beam displacement at the free end can be calculated based on the physics of the model. Backward simulation is the opposite working in reverse from the displacement of the free beam in a data driven approach. In this case several combinations of forces in locations will be generated that all will result in the same predefined end of beam displacement. Thus, in summary forward simulation transfers knowledge from known inputs to generate outputs, while backward simulation takes the outputs and forms potential inputs.

Furthermore, now that forward and backwards simulations have been defined, looking at the next steps in Figure 2-1 there is a High Fidelity (HF) and Low Fidelity (LF) simulations that occur. The creation of HF simulations is through the used of advanced computer aided simulation software's that can replicate real world physics and physical characteristics in

extreme detail and accuracy. These simulations are often very accurate but take extensive resources and time to complete their analysis the scales with the complexity of the models. In contrast, LF simulations are much quicker and less resource intensive [77]. This is due to LF simulations often being a simplified version or model of the real-world application. This can be done by representing the real-world physics and model in more simple shapes or equations that produce similar results to the real world and HF models, such as beam elements in [75]. These combinations of forward/backward simulation and High/Low Fidelity, create 4 sets of pairs that are used for each phase of LIVE's Learn, Identify, Verify, Extend methodology which will be explained further below as described in [9], [12], [14], [74], [75], [76].

Learn is the first phase and it begins with HF forward simulations. This takes theoretical analysis, experimental data, and advanced simulations to understand behaviours of the system. This is the phase where the important parameters are identified through expert knowledge to know what is important in the system to monitor. This is important to replace a large portion of the physical testing with accurate simulated results and reduce the amount of time for development especially in cases where experimentation is very costly. The types of critical components that can be analyzed but are not limited to include rotating shafts, seals, couplings, impellers, etc, this helps to determine failure signatures. These signatures include common failure sources like bearing flexibility, excitations, misalignments, cracks, and micro-fractures. The resulting data forms a foundational knowledge base for calibration between the real world, HF and LF models as well as training models for ML in later phases.

The next phase Identify now looks to complete the simplified system modeling using LF forward simulations. This involves taking the information that was learned in the HF model and targeting the key areas of analysis. The trained model and expert understanding gained during the learning phase are used to validate the LF model, which often is constructed using Simple Structural Beam methods. The LF model developed is made to match the HF models output in all the key features. The low fidelity can then be used for sensor placements and are determined based on analyses of the critical failure signatures and the

suitable number of sensors are chosen. During this phase, key indicators such as unbalance response, transient events, and system stability are identified.

The Verify phase begins the collection of data using sensors placed at the identified points on the physical system in the previous identify phase. The collected data is used to continuously measure and evaluate the health of the system and to calibrate and verify the results from the learn and identify stage. Once the data that is collected is verified with the LF model it will continually monitor the data and check it with backward simulation. The LF model will then constantly be checking the health of the system strictly from the feedback from the sensors. It can then identify the health of the system and any potential faults that may occur.

Finally, the Extend phases main goal is to prolong the useful life of the system or machine. This is done by taking the information from the verify phase and the LF model and performing the backwards HF simulation of the data received. From this the health of the system can be confirmed and the planning and executing of maintenance tasks can be completed based on the verified failure patterns. Using HF backward simulations and historical data, the system recommends specific interventions based on the errors it is seeing such as excessive bearing vibrations. The importance of this phase is the communication between the real model, the virtual LF model, and the HF model to notice changes and failure points and identify what those may be. The use of IoT and ML devices can simplify and improve this process.

LIVE DT methodology described is an effective structure to follow when producing a DT system. This methodology is followed in the following chapters and described as each step is taken in the analysis and development of a DT for a Rotary Machine system.

2.8 Bearing Analysis

Bearing rolling element bearings are major components of many machines and mechanical systems that support rotating shafts while also minimizing the friction from high rotational speeds. In many applications bearings can be a critical point in the operation and need to be monitored or swapped for efficient running [78], [79], [80].

2.8.1 Bearing Defects

In many DT applications failure data is an important portion of the research and this is especially true for bearings. One method studying bearing faults is to intentionally create faults through seeded defects, they create defects such as pits, spalls, or rectangular cutouts and then proceed to study the vibration or acoustic behavior of these bearings [81], [82]. The size of the damages can range from extremely small 0.2 mm^2 to large spalls of 500 mm^2 and are summarized in [78], [81], [82], [83], [84]. Research pertaining to ball defects are similar to defects as the inner and outer rings. In literature, some typical defects can be seen in Table 2-3.

One of the methods that are used to represent bearings is through stiffness. Stiffness is good indicator of health in many systems as bearings can easily be represented in a physical system as a support connected to ground using a spring and damper [85]. The dampening is highly nonlinear and complicated to model in HF but can be modified in the LF models. The spring portion of the bearing considers the stiffness of the system making it a good method for analysis.

Table 2-2: Seeded Damage from Literature.

Measurement	Bearing Type	Damage Seeded with	Seeded Damage	
Acoustic emissions	01B40MEX Split Bearing	Electric engraver with a carbide tip	Smallest Defect 0.2 mm² (circle) Largest Defect 108 0.2 mm² (rectangle) (depth undefined)	[73]
Frequency	Koyo 1205 double row self-aligning ball bearings	Electric spark erosion for line spall Electric etching pencil for rough surface defect	Fault [Length, Depth, Thickness] Spall Line [7.5mm, 0.3mm, 0.8mm] surface area = 6 mm² Extended rough surface/spall [7.5mm, 0.3mm, 16mm] surface area = 120 mm²	[74]
Vibration	SKF SY J 25 TF	Electro Discharge machine with wire width of 0.25mm	Fault [Length, Depth, Thickness] Inner Race 50% [30mm x 2.2mm x 0.25mm] Inner Race 75% [30mm x 3.0mm x 0.25mm] Inner Race 100% [30mm x 3.8mm x 0.25mm] Outer Race 50% [14mm x 1.4mm x 0.25 mm] Outer Race 75% [14mm x 1.8mm x 0.25mm] Outer Race 100% [14mm x 2.2 mm x 0.25 mm]	[75]
Frequency	Torrington 208-K bearing	Not seeded Damage – but disclosed results of damage from a run to failure test	Inner Race [252, 267,569] mm² Outer Race [28, 21, 25] mm² Roller [38] mm² (depth undefined)	[76]
Frequency	SKF 1207 EKTN9/C3	Seeded damage on inner and outer race	Inner Race 0.9mm (diameter) Outer Race 1mm (diameter)	[77]

Table 2-3: Ball Bearing Tests from Literature

Bearing Type	Damage Seeded with	Seeded Damage	Reference
Torrington 208-K	Not seeded Damage – but disclosed results of damage from a run to failure test	Roller [38] mm2	[76]
~	Run to Failure – no seeded damage	Flaking is observed.	[86]
~	Seeded rolling element damage using electro discharge machine.	0.1778, 0.3556, 0.5334 mm on rolling element	[87]
SKF6318	Real Field Defects	Three different health states (healthy, Multiple Defects, Outer Race defect) No dimensions given.	[88]

2.8.2 Bearing Testing from Manufactures

Manufacturers of bearings do not often share very detailed information on their test plans, but some literature shows some of those processes. In [89] released a quality standards guide for their suppliers. In this article, they follow the ISO 9001:2015 requirements [90]. This iso standard is a management standard and does not disclose specific test cases about their quality control. The range of testing they mention includes but is not limited to durability testing, contaminants, corrosion, friction torque, and material compatibility tests. They also test in high-pressure test rigs where they can generate 3000 bars of pressure in addition to large temperature ranges going as low as -40°C and to as high as 150 °C [22]. Another company specializing in rolling bearings use eddy currents to for quality control of the surface layer of bearing rings. They use the PVK-K2M and can detect defects such as burns, cracks, and other surface defects [91]. This company [92] use a variety of testing methods from vibration analysis, noise testing, durability testing. They claim that vibration diagnosis is the most reliable method for identifying bearing damage especially in the earlier stages. Vibrations can affect the performance and health of mechanical systems by transferring vibration to the environment and causing defects.

According to ISO 15242-1-2015, vibration can be measured radially or axially depending on the bearing type [93]. The velocity signal can be analyzed in one or more frequency bands. The bands depend on the rotational speed of the shaft/spindle. ISO 15242-1-2015 presents a general frequency band at 1800 RPM; the frequency range is between 50Hz to 10 000 Hz. But other studies suggest they can further be filtered into the following three: Low: 50-300 Hz, medium: 300-1800 Hz, and High: 1800 – 10000 Hz [92], [94]. But these bands are subject to change based on the shaft speed. Various sensors can be used from Displacement sensors to velocity, acceleration, and force sensors, but most available industrial devices use electro-dynamic vibration velocity sensors [94]. This is because rolling elements emit a wide spectrum of frequencies. Vibration displacement sensors struggle with high frequency amplitudes while acceleration vibration sensors miss the lower frequency amplitudes. Signals that are provided as velocity provide better resolution over a wide frequency range [93]. Despite the challenges it is possible to use acceleration sensors it is also likely that acceleration sensors will capture the absolute vibration of the bearing and the entire system it's mounted on.

Chapter 3. Methodology

The following chapter covers the design of the physical test system used for the completion of the thesis. The first Section 3.1 will talk about the initial design intentions looking at all the potential features that could be added, and the variables that were explored for a DT system. This is important for the design of a system that can be compatible for DT applications in future work. Furthermore, section 3.2 will look at the simplification of the design as the thesis research went on into its final form. The following section 3.3 will look more deeply at the selection and building of the system components. The final section 3.4 will focus on the sensors that were used for either the collection of data for use in the analysis of the thesis or for the validation of the system to be running without any issues.

3.1 Rotary Machinery System

A high-level testing plan was devised to map out each of the sub systems that were going to be implemented into the prototype. Figure 3-1 represents the block diagram for a sensor-based data acquisition and system for a rotary device. The system starts with a Rotary Device which will be the input of the system that will incite changes and act as any system would in industry. The input of the system is then to be influenced by testing variables that could be seen in any industrial system and could impact the results. These variables consist of items such as speed (rev/min), loading conditions like being overloaded or unbalanced loading, or other unexpected items such as misalignment, loose connections [95]. To monitor these changes to the systems sensors are needed to collect real-time data from the rotary device. Some of the common sensors seen used in industry and other literary works include voltage/current measurement, temperature, vibrations, displacements, or even audible differences [37]. For DT systems live communication of information between the actual system being monitored and the virtual system is necessary for the functionality of the DT. This communication is done through a microcontroller which establishes a connection between the sensors and the central processing unit which is a base computer that will handle any intensive simulations. This base computer is where the data is analysed and stored. Once the data is ready it is fed to the DT to diagnose the health of the system and prescribe maintenance plans.

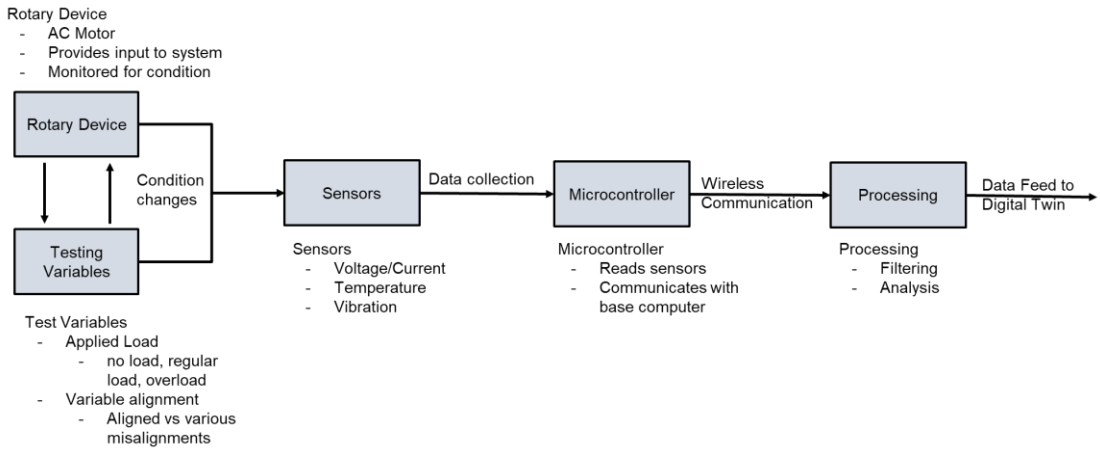

Figure 3-1: High level Architecture of Comprehensive DT System for Rotary Machinery.

Figure 3-2 illustrates a mechanical system architecture involving a three-phase AC motor, a transmission system, and a generator or brake. The system's primary function is to transmit rotational velocity from the motor through a transmission mechanism to a generator or brake. The three-phase AC motor serves as the primary power source, providing rotational energy to the system. This energy is transferred through a transmission system where potential mechanical errors such as misalignment, dimensional, and geometric errors are induced on the system to emulate existing faulty cases found in the industry and literature such as misalignment or bearing damage [95]. This is where the focus of the thesis will be shown in later chapters. The generator or brake at the output end either converts the rotational energy into electrical power or dissipates it as heat which is another potential source of monitoring. A sensor network is employed to collect the relevant data for the various phases of LIVE DT.

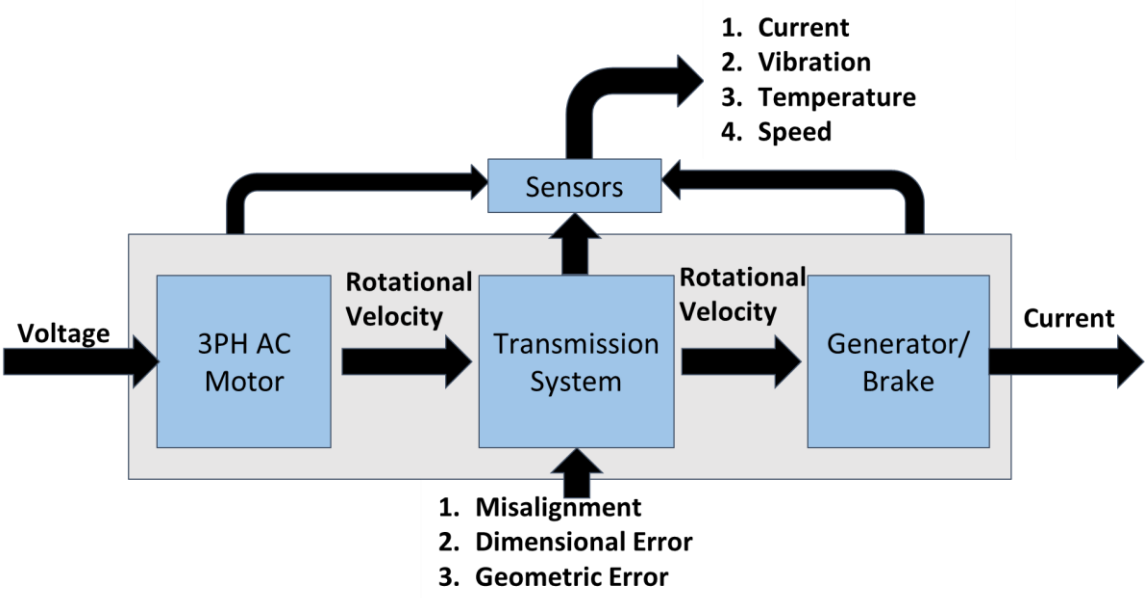

Figure 3-2: Architecture of Comprehensive Rotary System

An initial rotary machine system was drafted and set for construction as per Figure 3-3. In the design there are various components to be noted. The first is the motor which is the input of the system representing a motor, pump or other equipment in industry. This is connected to the transmission system that connects the motor shaft to a short shaft through a stiff coupling, that shaft is connected to a bearing for support and then a flexible coupling on the far end. The flexible coupling is meant to act as a buffer between the motor and the rest of the test set up to avoid any damage from being transferred to the motor from any effects further up the transmission line. On the other side of the flexible coupling is a longer shaft supported by a bearing and into a flywheel. The flywheel in this case acts as a movable object that can have additional mass added to it to create an unbalance in the system. Further on the line is a transmission system either a pully or gears system to be able to transfer motion onto the other parallel shaft. At the end of the first shaft is the Bearing Defect Inducer the focus of the thesis. This device is meant to impact movement on the system as if it was a regular bearing experiencing failures. On the other side of the pully is another support bearing and a generator that can be used to measure the output of the system in terms of energy generated. All the features in this test rig are supported by an aluminum rail system where each component can be moved and adjusted for different combinations and test positions making it modular future work additions.

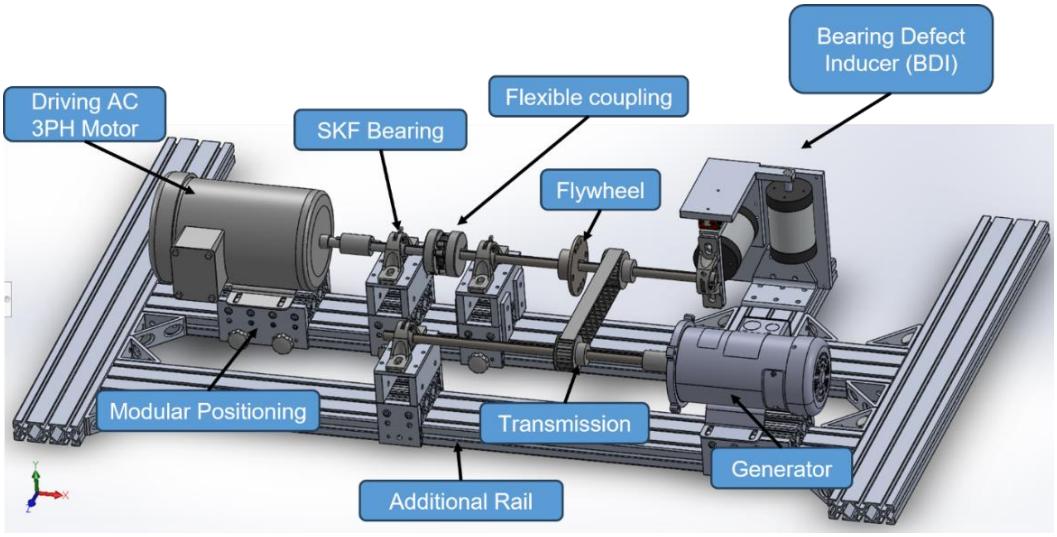

Figure 3-3: Comprehensive rotary machinery system

3.2 Bearing Focused Test Rig Design

A more focused model was drafted to validate the calibration phases between the various simulation fidelities required by LIVE DT for bearings. The system seen in Figure 3-4 now incorporates one three-phase motor attached to a long shaft through a stiff collar. The shaft then has 2 bearings, the first is to support the shaft right after the motor and coupling to ensure no major effects on the motor. The second bearing is attached to the final chosen BDI that will act as the input of error in the structure. The flywheel can be supplemented with hardware or components to create an unbalanced mass to also generate fault data or amplify the system vibrations. Like the comprehensive design it is modular with the ability to swap the order of the components and expand in future works.

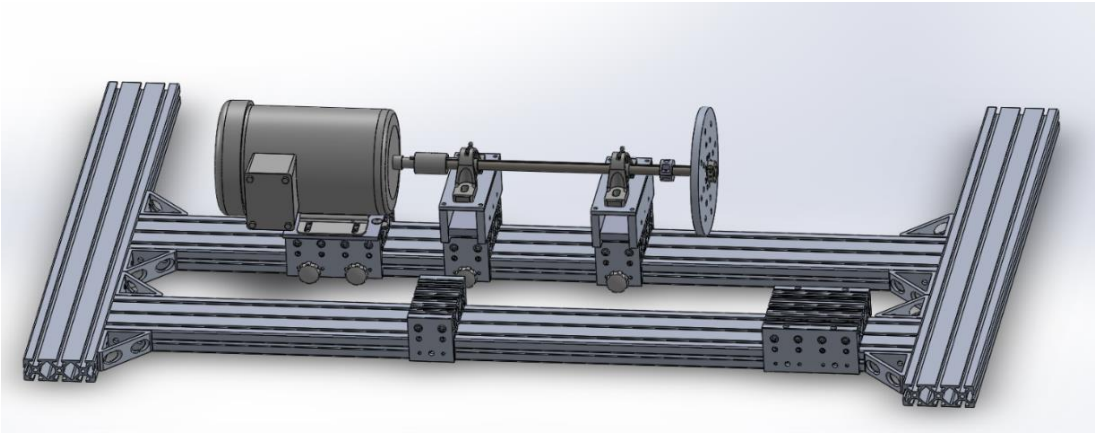

Figure 3-4: Bearing Focused Rotary Machinery System

3.3 Rotary Machine Sub-Assemblies and Components

3.3.1 Rotary Device

One of the most important parts of the rotary machine system is the motor itself. The motor selected for this research is an induction motor as they are the most common found in industries [79]. The motor in Figure 3-5 is a 1.5 HP (1.13 kW), 3-phase, 2 Pole induction motor. The motor is designed to run at a maximum of 3600 RPM, 60Hz for industrial applications. It operates at 230V or 460V with a rated current of 4.0/2.0 AMP, depending on the voltage configuration. For our configuration it is running at 230V based on the availability in our lab environment. The frame size is 56 which is used to create the mounting plate for the design. The motor was selected with a totally enclosed fan-cooled enclosure, ensuring protection against dust and moisture which is more than sufficient for our lab environment. This was decided to be suitable for our lab environment as it will not be exposed to outside or other harmful elements, in addition to being a standard enclosure for more rotary machine applications that do not require special circumstances such as waterproof casing. Additionally, the motor is CSA, UL & CE approved for safety considerations. More of the specifications can be read in the figure below.

Figure 3-5: Motor Selected for Testing

3.3.2 Motor Speed Control

An important element for the testing was the ability to control the speed of the motor. This was accomplished using Variable Frequency Drive (VFD). A VFD works by taking the supplied AC current and then converting it to a smooth and rectified DC voltage. The DC voltage can then be controlled using an inverter to toggle it rapidly known as pulse width modulation (PWM) to create an AC waveform. The controller can modify the frequency

of the signal making it variable and directly proportional to the speed of the motor. In this case the motor running 60Hz would be at a full speed of 3600 RPM, whereas 30Hz is half speed at 1800RPM. The ability to have control is an important parameter for the testing of the system and can be seen in the Figure below.

Figure 3-6: Mollom 1.5KW, 2HP Variable Frequency Drive

3.3.3 Flywheel

When deciding on potential testing options for the rotary system there were many potential faults to analyze. On consideration was to have a flywheel that can add additional weight to the system and act as an unbalanced mass if modified. In the final design the fly wheel is the component at the end of the shaft held in place by 2 shaft collars. The fly wheel is manufactured from Aluminum 6061T6 to be strong but also light weight as to not impact the system too heavily. The flywheel is 8 inches in diameter and 0.5 inches in thickness with a total mass measured at 1.051kg. This mass is needed for future calculations in the low and high-fidelity models and can be seen in Figure 3-7. The face of the flywheel has 3 rings of 8 holes set at 1-inch intervals from the centre of the flywheel up to 3 inches. This allows for the customization of adding masses at different lengths of the flywheel changing the centrifugal force *Fc* according to Equation (3.1), as the force is directly related to the mass *m* of the object at *r* radius from centre and where *RPM* is the rotational speed of the motor.

$$Fc = mr(\frac{\pi \times (RPM)}{60})^{2} \quad (3.1)$$

Figure 3-7: Flywheel for Rotary System

3.3.4 Bearing

The bearing selected for this test is a simple pillow block bearing manufactured by SKF in Figure 3-8. This bearing locks onto 5/8-inch shaft via a set screw and is sealed to not allow any debris or dust in as well as being pre lubricated for smooth rotation. Some of the key specifications important for this bearing included in Table 3-1. The load ratings are important to consider so that they are not experiencing forces that would cause failure, the same can be said about the limiting speed is higher than that of the motor and the weight is important for calculations in the design of the BDI as well as simulation results.

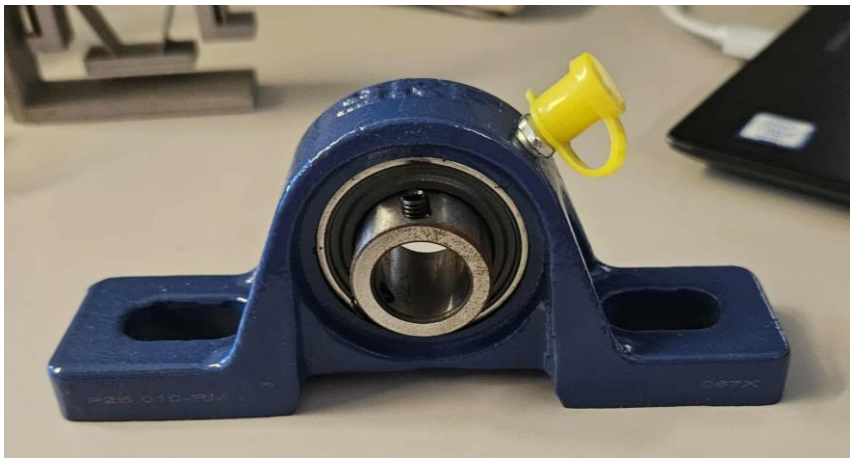

Figure 3-8: SKF P2B 010-RM Pillow Bearing

Table 3-1: SKF P2B 010-RM Pillow Bearing Specifications

Bearing Specification	Values
Basic dynamic load rating	9.56 kN
Basic static load rating	4.75 kN
Limiting speed	9 500 r/min
Weight	0.477 kg

3.3.5 Sensor Technology

Sensors have significant role in DT systems their uncertainties and resolutions dominate the overall accuracy of DT predictions and also the sampling strategy and data collection method strongly impact on the results of analysis [96], [97], [98], [99], [100]. The following provide a summary of the employed sensors.

3.3.5.1 Tachometer

A Hall effect sensor is a widely used tool for measuring RPM (revolutions per minute) in various applications, especially in motors and rotating machinery. This sensor works by detecting changes in magnetic fields as a magnet or magnetic material passes by the sensor with each rotation. When the magnetic field interacts with the sensor, it produces a voltage pulse, which can be counted and timed. By measuring the frequency of these pulses, the system can calculate the RPM of the rotating object.

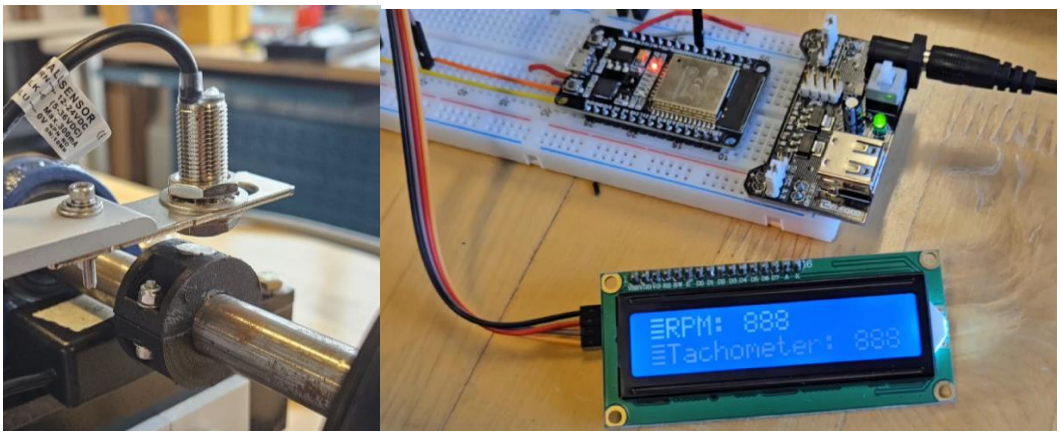

Figure 3-9: Sensor Devices for Speed Measurement
a) Hall Effect sensor and magnet b) LCD displaying RPM measurement readings.

3.3.5.2 Accelerometer

The LIVE DT communication between the physical and virtual domain is established with the effective use of accelerometers. The data from the physical model is the input for the HF and LF simulations. This data is acquired using KX134-1211 Tri-axial accelerometer that is placed directly below the bearings and at the motor as seen Figure 3-10. These 3 accelerometers collect the vibration data at the motor and each of the bearings to measure the impact across the system.

The data can be seen represented in graphical formations for analysis to understand the system and its reaction to any tests being completed. Typically vibration sensors are in the time domain and require Fast Fourier Transform (FFT) to convert the give the measurement of acceleration into the frequency domain [101]. Due to the sensitivity of the sensor not being sufficient the amplitude was taken for intervals of motor speeds, and the peak amplitudes were determined to be the natural frequencies.

Figure 3-10: Accelerometer Location
a) Placement Under Bearing b) Sensor in Casing

3.3.5.3 Current Sensors

An important feature to monitor is the three-phase phase induction motors current. This is helpful as another input parameter for our analysis in determining the health of the system. The diagram below represents a current measurement system for a three-phase induction motor driven by a Variable Frequency Drive (VFD). The power supply provides energy to the VFD, which controls the motor's speed by adjusting the frequency and voltage of the supplied power. To measure the current flowing to the motor, three current transformers

for each phase are placed on the output of the VFD. These current transformers capture the current signals and send them to a signal conditioning circuit, which processes the signals into a format suitable for further analysis. The conditioned signals are then sent to an Arduino, which digitizes and processes the data. Finally, the Arduino microcontroller reads the analogue current and transmits the data as a data stream, which can be used for monitoring, and further analysis of the motor's performance and behaviour. This setup helps in real-time current monitoring, fault detection, and PdM of the three-phase motor operating under a VFD. Figure 3-12 presents the test setup with the inline current transformers measuring the current from the VFD. Additionally, a clamp on the current sensor was used as a comparative baseline to ensure that the results that we were getting were accurate and correct to a trusted reference.

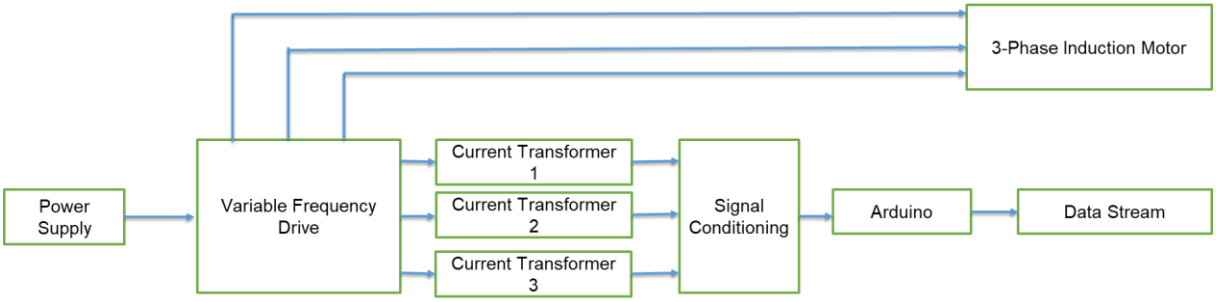

Figure 3-11: Current Sensor Measuring Architecture.

Figure 3-12: Testing of current sensor accuracy using clamp on meter.

Figure 3-13 is an analysis of three-phase electrical currents using the current sensors described earlier. The left side contains summaries for Phase A, Phase B, and Phase C

currents, including their mean values, standard deviations, and upper/lower bounds. The analysis confirms that no outliers are detected, indicating stable operation. The right side shows a plot of the three currents, where Phase A (blue) has a slightly higher mean current (2.15 A) and more fluctuation compared to Phase B (orange) and Phase C (green), both around 2.05 A and 2.04 A, respectively. The small standard deviations (0.01 A) suggest minimal variation, and the balanced current values indicate a healthy three-phase electrical system with no significant abnormalities. The small deviations in the graph can be correlated to the accuracy of the sensor used and are not of major concern as they are within expected deviations. The use of the sensor data as of this point was to ensure normal operating conditions and no abnormalities. Future work to improve upon the fault detection would also look to include the sensor data in addition to excessive temperature readings.

```
Phase: Phase A Current (A)
Mean: 2.15 A
Standard Deviation (σ): 0.01 A
Lower Bound (6σ): 2.07 A
Upper Bound (6σ): 2.23 A
No outliers in Phase A Current (A)

Phase: Phase B Current (A)
Mean: 2.05 A
Standard Deviation (σ): 0.01 A
Lower Bound (6σ): 1.97 A
Upper Bound (6σ): 2.14 A
No outliers in Phase B Current (A)

Phase: Phase C Current (A)
Mean: 2.04 A
Standard Deviation (σ): 0.01 A
Lower Bound (6σ): 1.97 A
Upper Bound (6σ): 2.12 A
No outliers in Phase C Current (A)
```

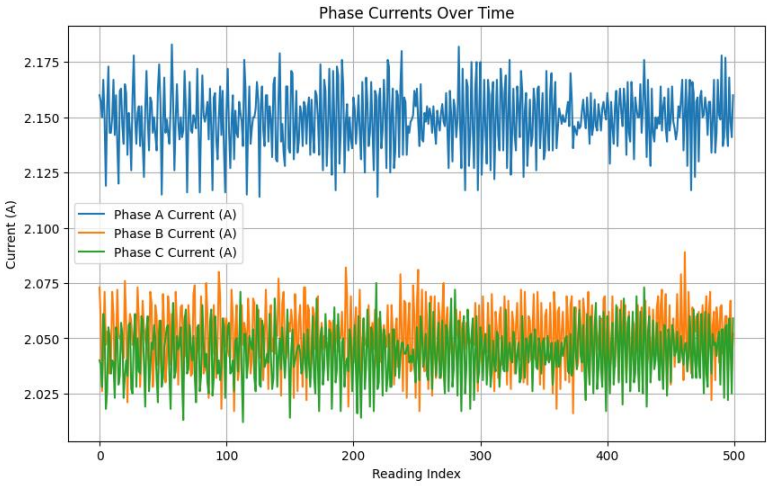

Figure 3-13: Current analysis for any faults and deviations.

3.4 Bearing Defect Inducer

In DT systems the primary goal is to predict failure, understand what is causing a failure in a system and attempt to prescribe the best method to fix or slow the wear of the item in question. The difficulties that come with this task are the need of failure data to be used in prediction be it through standard remaining useful Life (RUL) strategies or ML. The goal of the Bearing Defect Inducer is to focus on one part of the system and develop a method to artificially create failures in the system that can represent the component in question. The aim was to create a system that can produce a defined range of failure data from healthy to unhealthy conditions that can be measured reliably and repeatedly. The main strategy in

designing such a system is to reduce uncertainties and define the measurement method with minimal cross-sensitivity [102], [103], [104], [105], [106].

In this case we wanted to investigate a simple bearing and the ways we can create changes into the system that could represent healthy and unhealthy conditions.

3.4.1 Voice Coil Actuator

The first concept explored is using a bearing attached to an actuator. The goal of this approach is the creation of a mechanism to move the bearing to create a movement pattern that would match the movement pattern of a defective bearing. When studying bearing defects there can be many different types a bearing might experience.

The studies in [81], [82], [83], [84], [107] show many types of bearing damage as well as creating their own damage into their inner and outer races of the bearings. They feature circular, lines, and rectangular defects, defects are etched or scratched into the surface of the inner or outer race. Surface area is the focus of study in literature and can range from $0.2mm^2$ to $569mm^2$. The depth is also arbitrary and depends on the study with some defects are only 0.3mm while another study studies a maximum depth of 3.8mm. Therefore, in the instance that a bearing might have a pitting or denting it could cause micro movements in the directions of the defects. With an actuator the aim would be to replicate the defect by moving the bearing in the direction of a theoretical defect. For this to be an effective strategy the actuator would need to meet the following criteria.

1. Support the weight of the bearing
2. Move in the vertical and horizontal axis for a 2D circular path
3. Actuate at a speed fast enough to replicate at least 1 defect path per revolution
4. Accurately and consistently replicate the displacement action

To try and reach these criteria the most suitable actuator that could be found were voice coil linear actuators. The voice coil actuators could be configured so that each one acts in a different axis plane. The first Actuator would impose horizontal movement on the second actuator and then the second actuator would then impose vertical movement on the bearing allowing for 2 axis movement allowing for the creation of a defect in any direction. The preliminary design of a potential actuator that was looked at can be seen in Figure 3-14 a).

In the same Figure 3-14 b) it shows a theoretical trajectory of a single point on the shaft. The blue line represents and normal undeformed path, whereas the red path represents the path when there is a defect in the bearing that causes the path of the shaft to slightly differ. This path could be emulated by the proposed bearding defect inducer.

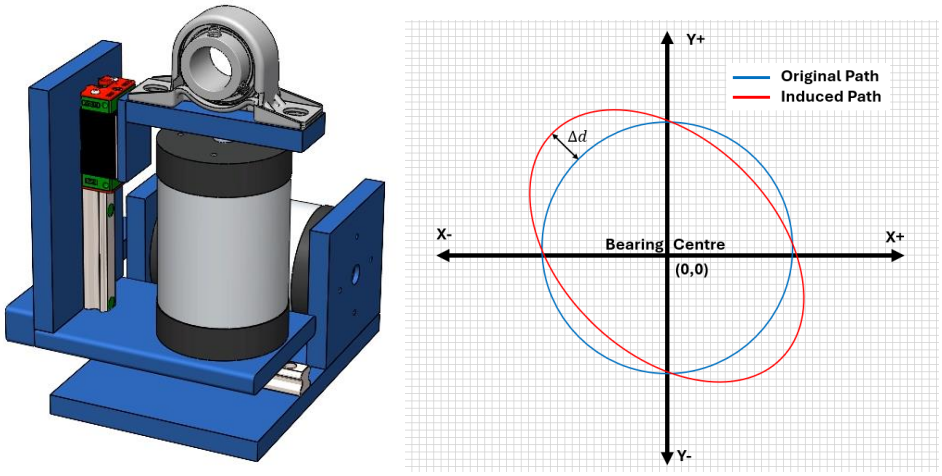

Figure 3-14: Voice Coil Actuator
a) 2 Stage Voice Coil Actuator with Bearing b) Voice Coil Motion Profile

One of the concerns with this design was the displacement of the deviation of the defect. As seen in the articles the defects can be small and the concern with the voice coil was the ability to accurately achieve these displacements. When researching potential options on the market it was determined that there were 2 deciding factors in stopping this method of approach. The first issue was the displacement. For high precision voice coils there are not many options that are able to meet the 3 criteria of capable force, frequency, and displacement. An example of a voice coil used is [108] with the important specifications seen in Table 3-2

Table 3-2: Voice Coil Specifications

Specification	Values
Stroke Length	**12.5 mm**
Force at 100% duty cycle	**80 N**
Displacement Resolution	**~6 µm***

With an estimated combine mass of 1.5kg between the bearing and the flywheel and the additional 1.5kg – 3kg for the actuator that will hold the most weight the total mass moved is 3kg to 4.5kg. Calculating the minimum force *F* required to hold the mass newtons 2nd law is used from Equation (3.2) where *m* is the total mass and a is the acceleration. In this equation the acceleration is calculated by the following formula for triangular acceleration.

$$F = ma \tag{3.2}$$

Since force was meet the next concern was the displacement and response time. When analysing the capability of the voice coil system the following Equation (3.3) can describe the acceleration profile. In this equation variable *d* represents the distance moved, *t* is the time to complete the move, and *G* is the gravitational constant. Doing a sample calculation assuming a distance moved of only 0.3mm as defined in some of the smaller tests described in literature earlier, *G* being 9.81m/s^2, and time *t* being defined as one over the motor frequency *fm* (one revolution) divided by 2 to complete the full actuation forward and backwards Equation (3.4) the given acceleration is 1.78g [109].

$$\alpha = \frac{4 * d}{t^2 * G} \tag{3.3}$$

$$t = \frac{1}{fm * 2} \tag{3.4}$$

To properly control the output motion profile, a control loop would be needed. In enacting this control loop the control system requires the acceleration to be 10g or less which is achieved. Next using Equation (3.2), the required force can be calculated in the worst case of 4.5kg total weight of the system, and an acceleration of 1.78g's to be 78.55N which is barely under the force required without considering any factor of safety. In the case the overall weight would be less there would be more room for error but in this case, it is already only considering the smallest sized defect that would be tested. In addition, this is only capable of doing 1 defect and not multiple if required. Finally, the overall cost of this design would be severely expensive to implement and would take a significant amount of time to calibrate the control system to accurately perform the movements that would be intended and was not recommended to be feasible by the manufacturer of these voice coil stages. Thus, it was determined this would not be the approach taken.

3.4.2 Compliant Mechanisms

Another potential methodology is emulating bearing stiffness using a compliant mechanism or shape memory. They are found to be very useful applications for manipulating property materials to accomplish specific functions. Lees et al. (2007) [110] demonstrates controlling bearing stiffness using shape memory alloy with future works set. In this article [111] the author is able to make a mechanism that can change the stiffness of the system in a bidirectional output. This is useful to be able to change the stiffness of the system through simply geometry and material properties.

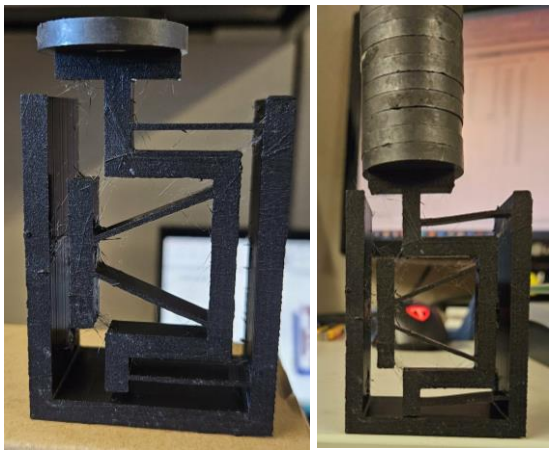

Figure 3-15: Compliant Mechanism Under Different Weights

This process was investigated for other states other then only 2 states of stiffness which can be seen in the following articles for variable stiffness mechanisms [112], [113], [114]. This was explored further as seen in Figure 3-16 using additive manufacturing to test print a compliant mechanism using 3D printed polylactic acid (PLA) in addition to stainless steel using Direct Metal Laser Sintering (DMLS). Print using PLA allows for quick prototyping and testing, while DMLS allows for the use of stronger materials to be used in the manufacturing of the compliant mechanism. The design seen in Figure 3-17 was modified from [110] with the goal of testing it in the side position with the top face acting as a

platform for a bearing in the future. The goal would be to have a mechanism that can toggle between a stiff (healthy) state and a loose (unhealthy state).

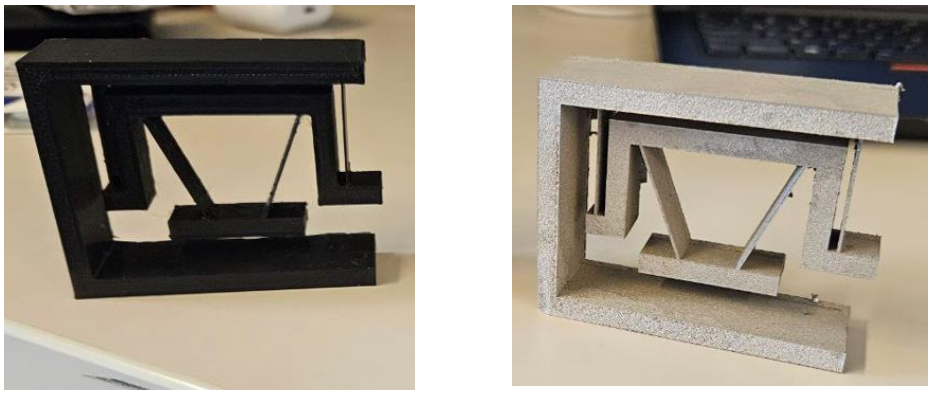

Figure 3-16: Compliant Mechanism Materials
a) Made from PLA b) Made from Stainless Steel

The design was further modified to have a screw and bolt to be able to variable control the stiffness of the system. Upon testing this to make this version of a BDI based on FEA simulations it was determined that PLA would be too soft a material and deformed too much over a small weight as seen in Figure 3-17 where it deforms nearly 2mm after half the bearing weight, not including weight of shaft.

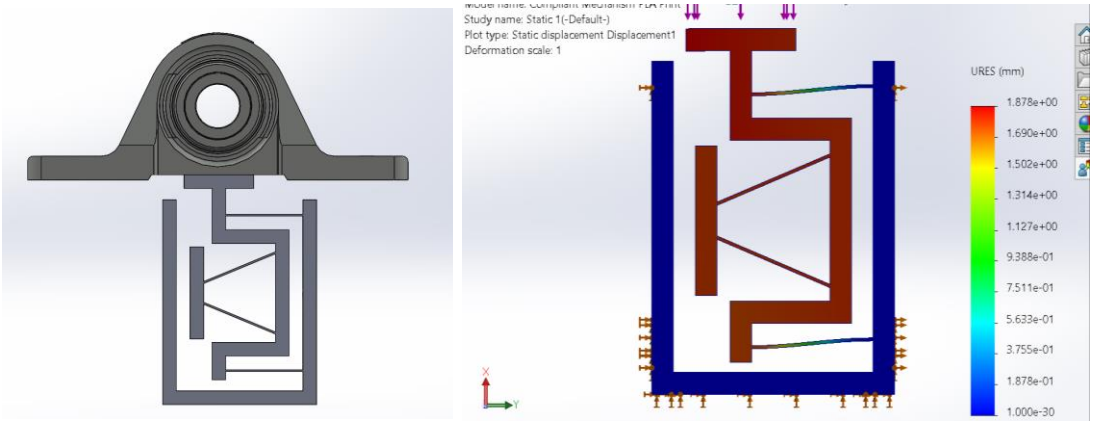

Figure 3-17: Compliant Mechanism Design
a) Bearing on BDI b) FEA of PLA Compliant Mechanism

In addition, to be useful in 2 DOF horizontal and vertically and have more than a binary state of stiffness variability it would make the shape very complicated as demonstrated in

[115] with the variations in design as well as Figure 3-18. It is also difficult to print using DMLS thus not making this method feasible.

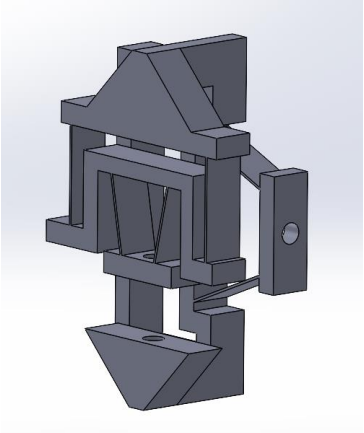

Figure 3-18: Potential Compliant mechanism Design for 2 DOF

The stainless-steel version was tested for its stiffness changes using a compression machine. The results showed that in the early elastic region the simulated and the actual test had similar stiffness curves. However, the design quickly started to reach the limit of its compression and was interfering with itself leading to the spike in stiffness in the 3rd slope in Figure 3-19. Despite having sufficient stiffness numbers, the complication in the printing process and complexity of the design needed made it no feasible but it could be a potential item to revisit for future applications.

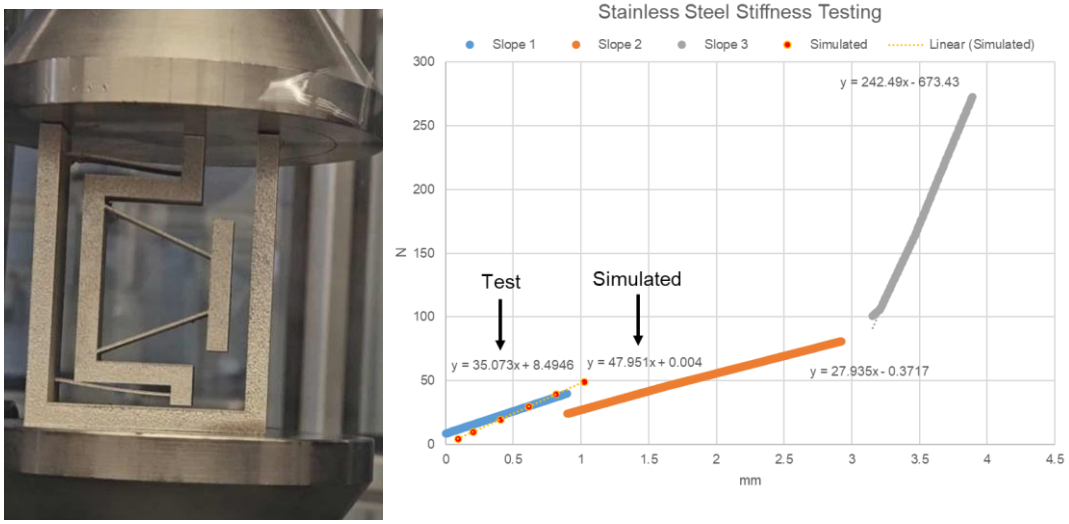

Figure 3-19: Stainless Steel Compliant Mechanism and Stiffness Testing Results

3.4.3 Stiff Beam Deflection

Another method investigated was the use of simple beam deflections. The theory behind simply supported beams is when a beam is not fixed but supported on both ends of the beam as show in Figure 3-20 the displacement that the beam see is already determined by a series of equations. Using these predefined equations, it is possible to get the stiffness of the beam from its deflection.

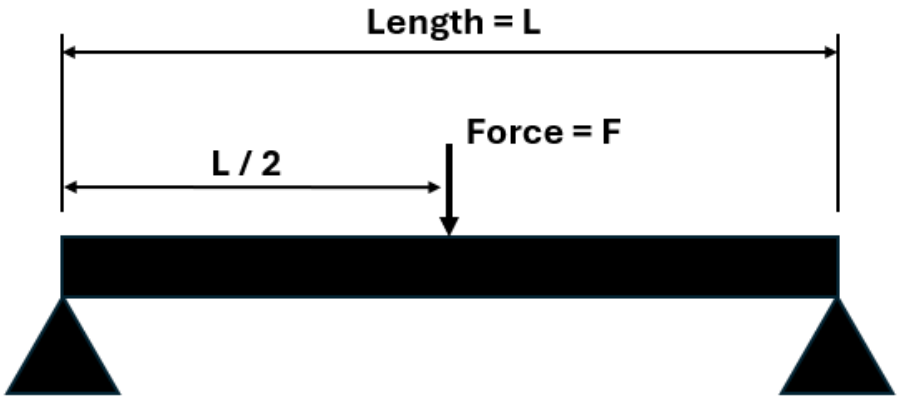

Figure 3-20: Simply Supported Beam with Concentrated Center Load

In this case the force is designated at the centre of the beam which will cause a deflection in the beam. Using this deflection and the force that is applied it is then possible to calculate the stiffness of the beam. In this scenario the deflection of the beam is described in Equation (3.5) [85]. In this equation F represents the force at the beams centre, L represents the length of the beam a from each of the supported ends, E is the young's modulus of the material, and I is the centroid or area moment of inertia and is defined by Equation (3.6) with r being the radius of a circular beam, this would change for a rectangular beam.

$$\Delta d = \frac{FL^3}{48EI} \tag{3.5}$$

$$I = \frac{\pi r^4}{4} \tag{3.6}$$

Using these equations, it is possible to design a beam that can have a desired stiffness. This was taken account into the design of BDI in Figure 3-21 where a bearing on a stainless steel plate is attached to the centre of a beam that is created using stainless steel using

DMLS. This beam is then seated into 2 adjustable V-clamps creating a simply supported beam structure at either end, while the bearing attached to the shaft will prevent it from and rotation. The V-clamps can be adjusted to move closer to the center where the bearing is, thus this will cause the deflection to decrease by a factor of L^3 but also inversely increase the stiffness of the system. This allows for a methodology of artificially modifying the stiffness of the bearing through the beam to test multiple failure conditions.

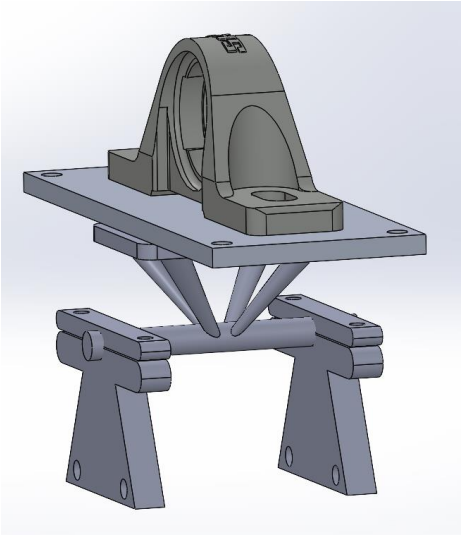

Figure 3-21: Stiff Beam Deflection BDI Design

In the case of bearing defects, it is difficult to reach the same level of stiffness since they are very high levels of stiffness. What can be done is that the level of deflection for known defects can be found and that can be emulated with this design. The clams can be pushed inwards for the stiffest condition and then they are moved outward to the most extended distance it can match the deflection of known defects discussed previously. An example of a case like this can be seen in

Table 3-3, in this case stainless steel is used since that is available with the 3D printer, max length is limited to the build plate of the printer and minimum length is limited by the interference with the central supports. The weight of the bearing and plates and be estimate out for this sample calculation. The beam radius was selected based on getting a sufficiently large enough displacement to match defects discussed earlier. The results of this are shown in Figure 3-22 where it is evident how changing the length of the beam affects stiffness and displacement. Although this method seems very effective in achieving the goal of

created failure sets this method was not fully approached due to the lack of availability of being able to manufacture the specialized beam component. This has potential for future work further exploring this methodology.

Table 3-3: Beam Deflection BDI Specifications

BDI Specification	Values
Max Beam Length	90 mm
Min Beam Length	42 mm
Estimated Mass (Bearing + Plates)	1.5 kg
Material	Stainless Steel
Young's Modulus	210 GPa
Beam Radius	2.5 mm

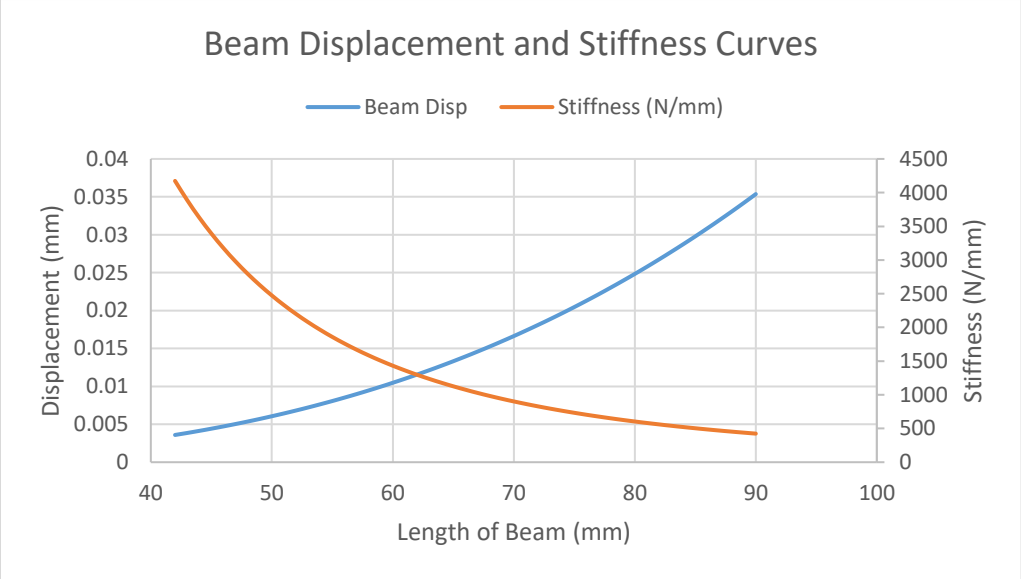

Figure 3-22: Beam Displacement and Stiffness Vs Beam Length

3.4.4 Spring Suspended Bearing

The last method that was explored and inevitably chosen as the optimal approach is using the compression of springs to simulate different levels of stiffness like the beam deflection method. This method was ultimately chosen as it is cost efficient and easily modifiable and changeable for the system to alternate between stiffness levels. The design below has a bearing on a stainless-steel plate suspended between 8 total springs, 4 below and 4 above as seen in Figure 3-23.

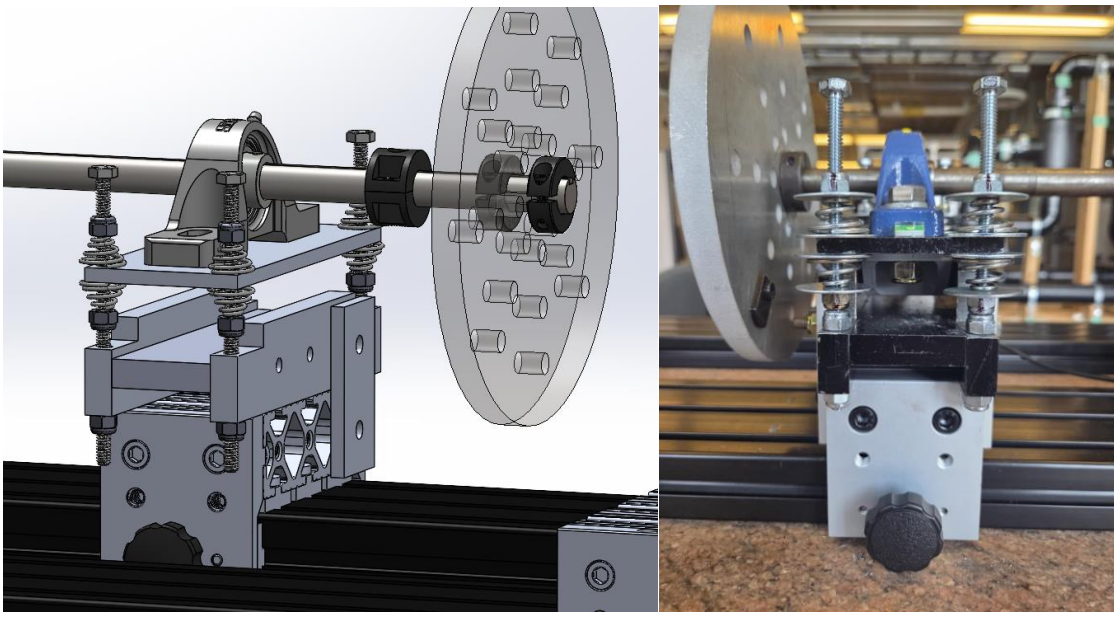

Figure 3-23: Spring Supported Bearing
a) CAD Model of BDI, b) Physical Twin BDI

These springs are connected in parallel to create an overall system with a large stiffness. The one consideration is that the use of conical springs is chosen to have varying stiffness along its compression. This will allow the connection between the spring length of compression to be tied to different levels of stiffness. Since the springs are conical and nonlinear and placed in opposite directions, the length of the top springs is not always equal to the length of the bottom springs. The overall stiffness can therefore be calculated as seen below, and since all the springs are the same, while in a stationary position the K_{total} is below with $k_1$being the stiffness of one spring and

$$K_{total} = k_{bottom\ springs} + k_{top\ springs} = 8 * k_1 \tag{3.7}$$

However, since the springs are conical and not symmetrical with the top set of springs being oriented in the opposite direction while in operation the stiffness of the system will flex. To find the stiffness of a single spring the following series of equations from Equations (3.8) through Equation (3.17) are needed to be solved. The variables and information needed to complete all the equations can be found in Table 3-4.

Table 3-4: Spring Variables and Specifications

Spring Variables	Meaning	Values
$\boldsymbol{L}$	Current Length of the spring	3.556 mm – 15.875 mm
$\boldsymbol{L_o}$	Uncompressed Length of Spring	15.875 mm
$\boldsymbol{G}$	Shear Modulus (302 Steel)	77.2 GPa
$\boldsymbol{d}$	Spring Wire Diameter	1.8288 mm
$\boldsymbol{n_a}$	Number of Active Coils	2
$\boldsymbol{D_1}$	Mean Diameter of Small End	9.2964 mm
$\boldsymbol{D_2}$	Mean Diameter of Large End	22.9362 mm
$\boldsymbol{L_a}$	Active Length	14.0462 mm
$\boldsymbol{L_s}$	Length at solid/ Ground	0 mm
$\boldsymbol{R}$	Constant Spring Rate in Linear Region	10935.19 N/m
$\boldsymbol{p_t}$	Force at Transition from Linear to Non-Linear	62.828 N
$\boldsymbol{L_t}$	Length at Transition from Linear to Non-Linear	10.129 mm
$\boldsymbol{P(L)}$	Force as a function of Length	See Below

First the Equations (3.8), is used to get the force as a function of spring length in the linear region by taking the uncompressed length of the spring L_0 and subtracting the current length of the spring L and multiplying it by the constant spring rate in the linear region R. This R spring rate is solved in Equations (3.9) using the shear modulus G, spring wire diameter d, active spring coils n_a, and the mean diameter of the small and large end diameters D_1, D_2 respectively. This makes up the initial part of the compression sequence.

$$P(L) = R\,(L_0 - L) \tag{3.8}$$

$$R = \frac{G\, d^4}{2\, n_a\, (D_1^2 + D_2^2)(D_1 + D_2)} \tag{3.9}$$

Once the linear portion of the spring force and length are found the nonlinear section must be found next using Equations (3.10). In this equation there are several variables that are needed to be solved first ranging from K_1 through to K_7. K_1 through to K_7 are equations that can be substituted to find the final spring force. In equation (3.16) and equation (3.17) L_a represents the active length of the spring, L_s is the length of the spring at ground or its fully compressed length. These are found in the following equations to eventually solve for the Non-Linear Phase.

$$P(L) = \left(\frac{K_1}{2}\right)^{3/2} \left\{1 - \left(1 - 2\left[1 - \left(1 + \frac{K_2}{K_1^2}\right)^{1/2}\right]\right)^{1/2}\right\}^3 \tag{3.10}$$

$$K_1 = K_3 - \frac{K_2}{3K_3} \tag{3.11}$$

$$K_2 = -\frac{K_6}{K_5} \tag{3.12}$$

$$K_3 = \left\{\frac{K_4}{16} + \left[\left(\frac{K_4}{16}\right)^2 + \left(\frac{K_2}{3}\right)^3\right]^{1/2}\right\}^{1/3} \tag{3.13}$$

$$K_4 = \left(\frac{K_7 - L_0 + L}{K_5}\right)^2 \tag{3.14}$$

$$K_5 = -\frac{2\, D_1^4\, n_a}{G\, d^4\, (D_2 - D_1)} \tag{3.15}$$

$$K_6 = -\frac{3}{8(D_2 - D_1)}\left(G\, d^4\, \frac{(L_a - L_s)^4}{n_a}\right)^{1/3} \tag{3.16}$$

$$K_7 = (L_a - L_s)\, \frac{D_2}{D_2 - D_1} \tag{3.17}$$

Upon solving for the linear and nonlinear regions to know when the transition between the 2 phases occurs the below Equation (3.18) solves for the force at transition P_T and Equation (3.19) is used to get the spring length at transition L_T. These equations are found at what force and spring length the transition happens at. Now the 2 equations for force as a function of length have their upper and lower bounds and the full spectrum can be made.

$$P_T = \frac{G\, d^4\, (L_a - L_s)}{8\, D_2^3\, n_a} \tag{3.18}$$

$$L_T = L_0 - \frac{P_T}{R} \tag{3.19}$$

The following are the results of the full spectrum stiffness analysis of a single spring in Figure 3-24. In this figure is a 5th order polynomial used as a line of best fit to estimate any point on the curve. It has an R-Squared value of 0.9982 signaling a significant prediction of the stiffness by the polynomial.

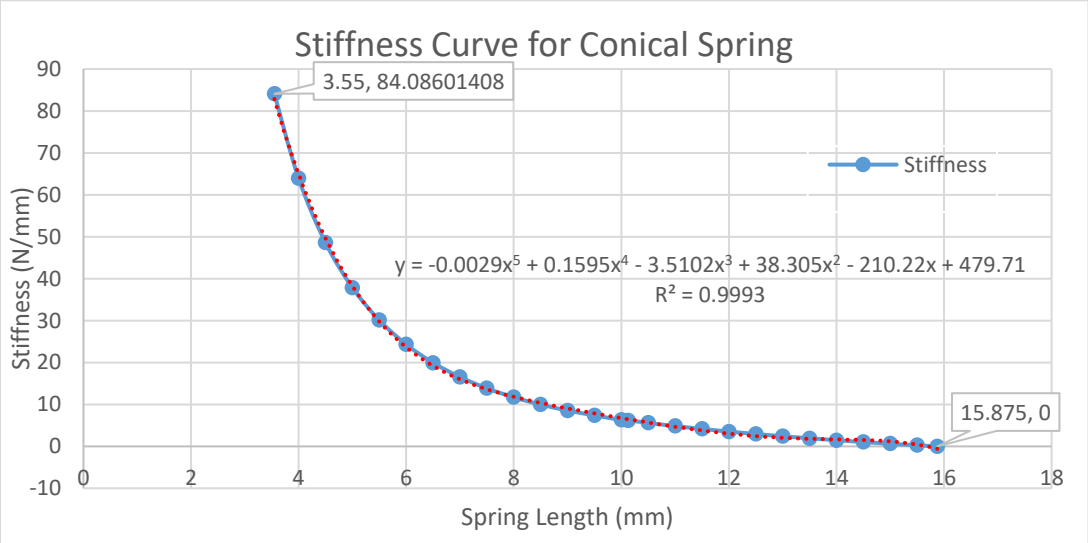

Figure 3-24: Calculated Stiffness Curve for Conical Spring

When considering the conical spring it reaches its max compression at about 3.56mm, the stiffness value can then be taken from this point as about 84.09 N/mm. When the system is at rest it was mentioned earlier that the stiffness of the system is measured as the stiffness of a single spring multiplied by 8 for all 8 springs in parallel, this results in an overall stiffness of 672.72 N/mm in fully healthy condition.

Now that the spring condition is understood actual testing of the physical twin could be done. The testing was done by first measuring the height of the untouched bearing to make sure when leveling was complete for the BDI bearing the correct height would be maintained. The nuts at each of the springs were then tightened until the springs were fully compressed. The height was then checked to ensure it was the same as the untouched

bearing and the level was tested as well. This can be seen in Figure 3-25. The system was then tested running at various speeds and measuring the vibration data. Then once different speeds were tested for at the current stage the nuts which held the springs in their set position would be loosened by 1 full rotation or by about 1.27 mm based on the threads used in this case. This was repeated until there was no longer any room to unscrew the nut, leaving the spring in its most free position.

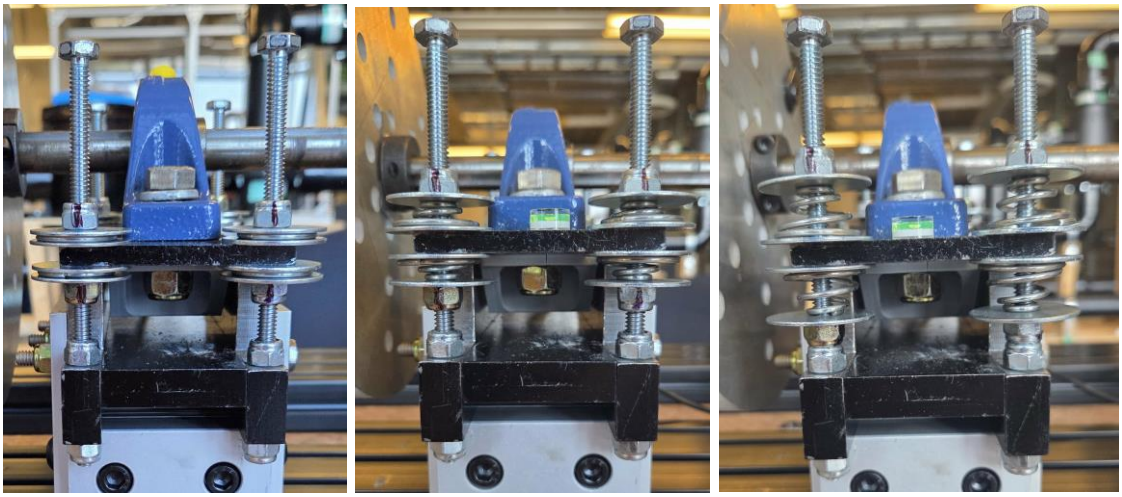

Figure 3-25: Stages of Spring Compression
a) Fully Compressed Spring b) Half Compressed Spring c) Fully Uncompressed Spring

Upon analysis at each level of the springs being loosened the vibration data was analyzed to find any characteristics of the system in terms of natural frequency. This can be found ad any peaks that are noticed in the data. For example Figure 3-26 shows the 100% healthy condition with springs fully compressed, in this image there is a steady increase in acceleration amplitude until about 27.5 Hz, here a noticeable peak can be seen as the amplitude drops back down for a few more samples afterwords. A summary of the recorded peaks for different levels of stiffness over multiple samples can be found in Table 3-5 and Table 3-6 below [96], [97], [98]. The data can be separated into 2 Distinct groups of frequencies with the first 2 in green signifying healthy condition and then the next groups seeing a large drop of in first natural frequency signifying that there is damage in the system and the bearing needs to be changed.

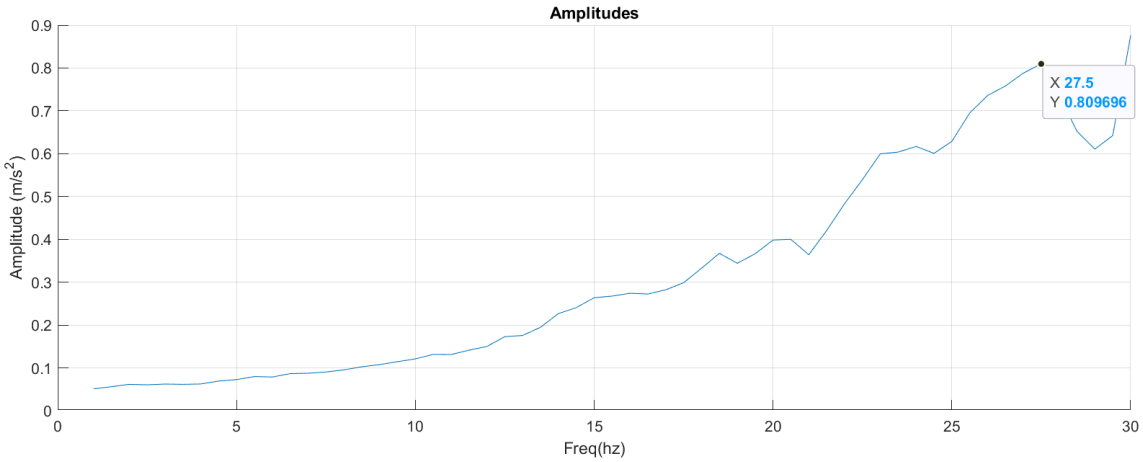

Figure 3-26: Vibration Analysis of Tested BDI at 100% health.

Table 3-5: Test data for first 5 Spring conditions

Spring Length	Test 1	Test 2	Test 3	Test 4	Test 5	AVG	High	Low
1.83	26.0	27.0	27.5	26.5	28.5	**27.1**	**28.5**	**26.0**
3.10	24.6	27.5	25.3	27.0	29.0	**26.7**	**29.0**	**24.6**
4.37	19.2	19.0	20.0	16.0	22.5	**19.3**	**22.5**	**16.0**
5.64	20.4	20.0	18.3	16.0	16.5	**18.2**	**20.4**	**16.0**
6.91	19.5	20.5	17.5	14.8	16.0	**17.6**	**20.5**	**14.8**

Table 3-6: Summary of Vibration Data Testing

Spring Length (mm)	Total Stiffness (N/mm)	Sq Root of Total Stiffness (N/mm)	Tested Peak Frequency (Hz)
1.83	672.72	25.94	27.5
3.10	672.72	25.94	27.5
4.37	364.05	19.08	19.5
5.64	202.35	14.23	18.5
6.91	123.76	11.12	20
8.18	80.79	8.99	15.5
9.45	55.32	7.44	15
10.72	42.08	6.49	14.5
11.99	28.36	5.33	14.5
13.26	17.26	4.15	11.5

Now that the vibration data has been acquired with respect to the stiffness based on the calculated spring length it is now possible to plot the frequency versus the stiffness. Before

this can be done it is important to note that the natural frequency can be defined by equation (3.20) [85]. This shows that frequency is directly proportional to the square root of stiffness over mass. Therefore, Figure 3-27 shows the linear relationship between the frequency and the square roots of the total stiffness of the system measured in Table 3-6, while showing a strong R-Squared correlation over 0.9. The deviations in accuracy can be attributed to errors and slight deviations in the test data, in addition to the nature of BDI causing the mass to shift during tests affecting the results.

$$f = \frac{1}{2\pi}\sqrt{\frac{k}{m}} \tag{3.20}$$

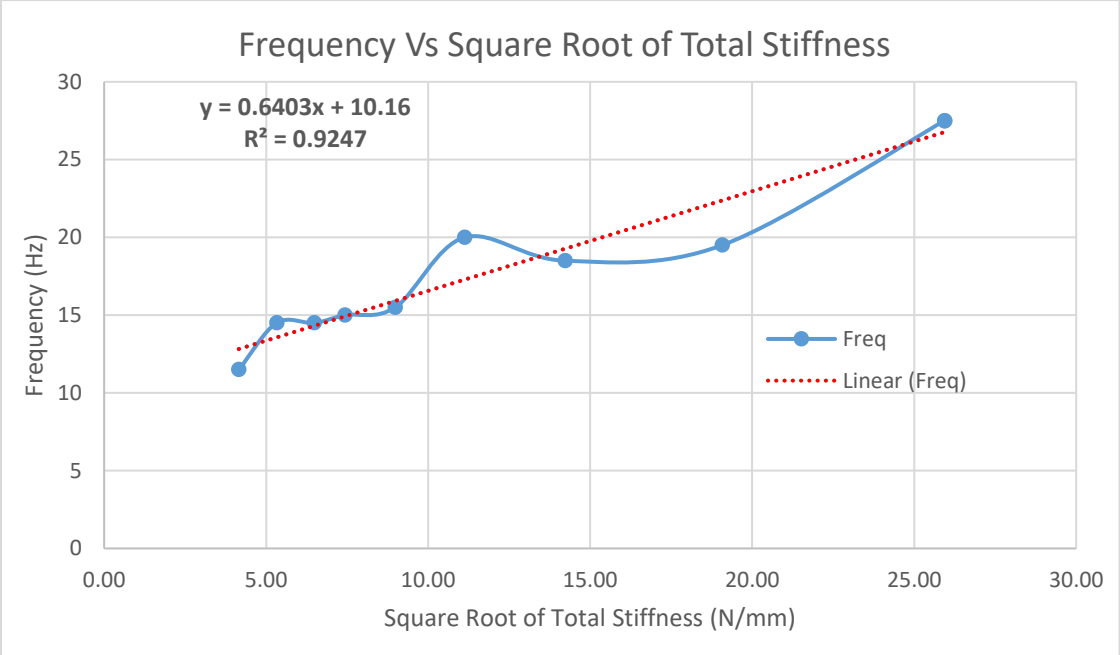

Figure 3-27: Frequency VS Square Root of Total Stiffness

3.5 High-Fidelity

The HF model created in for this analysis uses a computer aided engineering software to perform modal analysis on the twin of the physical model. The scale of the model is set to 1:1 scale and was created using CAD modeling software. The isometric view can be viewed in Figure 3-28 and a side view comparison of the digital model and physical model can be seen as well. The system as described from left to right is a 5/8-inch keyed shaft that extends through 2 bearings represented by the circular disks and finally connected to a

flywheel at the end of the shaft. The bearings represented by the discs are an incorporated feature of the software. All locations were set to match the current state of the physical twin. In addition, each of the components also have the proper materials applied such as aluminum for the flywheel and carbon steel for the keyed shaft and ensured that their core characteristics are the same such as mass.

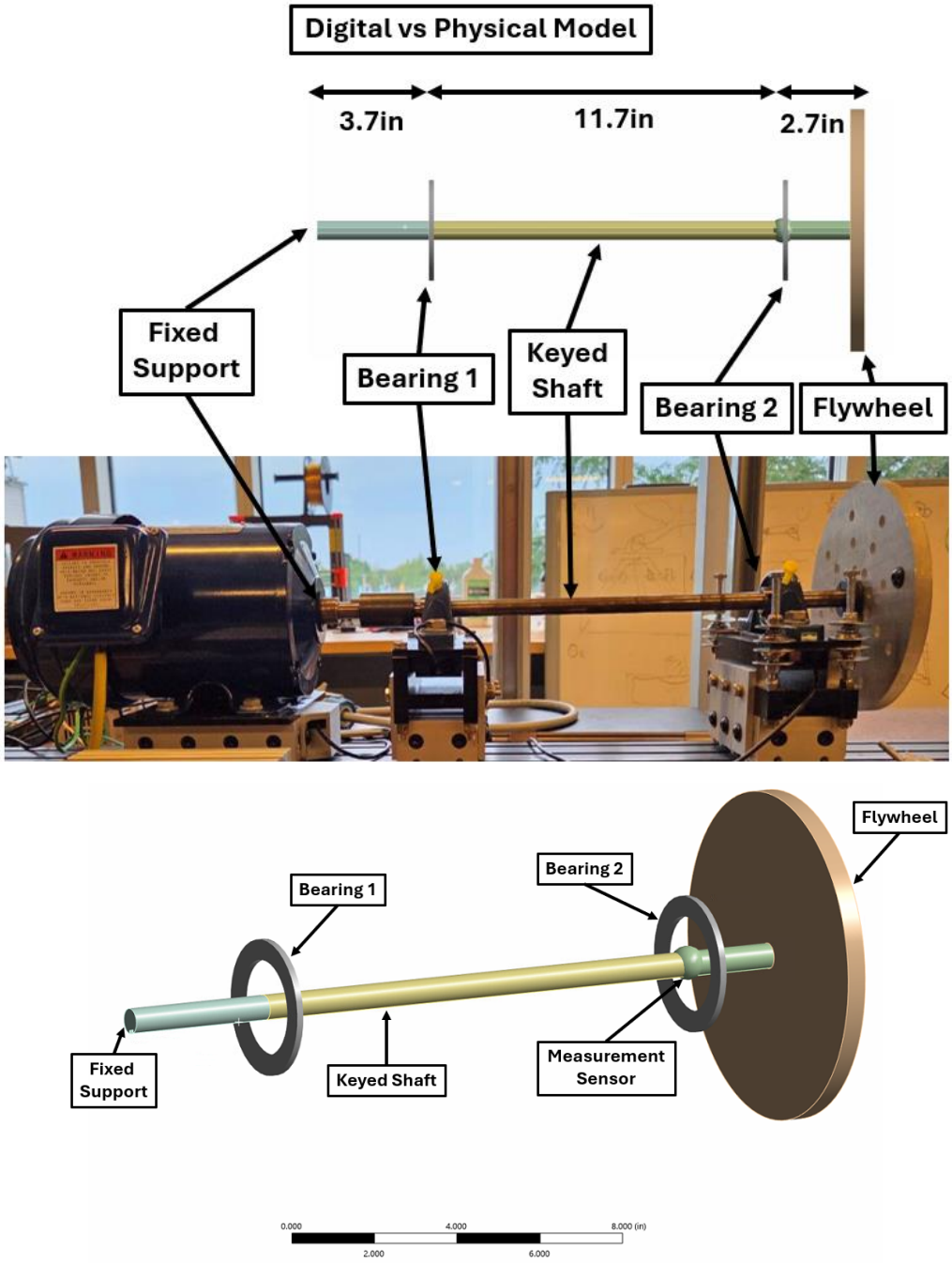

Figure 3-28: HF Side Profile Vs Physical Model b) HF Model Isometric View

Now that the DT is accurately recreated inside of the CAE software it needs to be prepped before simulations can begin. The first step is to consider what the boundary conditions to be set for this system. The boundary conditions are important to consider to accurately represent the system in the physical environment. The system makes contact in 3 locations; the first location is on the far left the open-ended shaft. On the physical twin this is seen to be connected to the motor directly, since they will not be the main concern of any of the changes and is considered the stiffest part of the system it is treated as a fixed boundary condition. This can be expanded on in the future and treated as a bearing since the motor has an internal bearing but for this experiment it was found that a fixed boundary condition was sufficient as the fixed healthy bearing to the right of the of the fixed support accounts for the stiffness to the left of the system. The other boundary conditions are defined by the 2 bearings in the system, when inserted as a bearing they are defined as ground to shaft solid connections by the system. Finally, no constraints are place on the end of the shaft or flywheel as those are hanging in out physical twin. The next consideration for the HF simulation is the defining of the mesh prior to modal analysis. As seen in [12], [116] the more detailed the mesh defined by its size, the longer the it takes to simulate. Since the model in this case is simple geometry, just a shaft and circular disk the default mesh size was deemed sufficient and used for the analysis and can be seen in Figure 3-29.

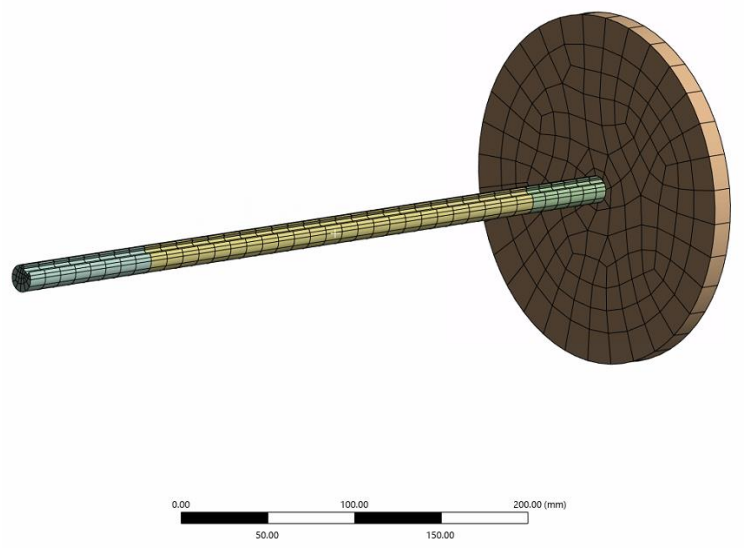

Figure 3-29: Mesh of High-Fidelity Model

The last item to set was the stiffness of the bearings which would be one of the focus points for changes in the system. The bearing stiffness is modified through 2 variable k11 and k22 and represent the horizontal and vertical components of the bearing respectively [117].

3.6 Low-Fidelity

The LF model aims to accomplish the same goal as the HF of replicating the physical twin. The advantages of LF model lie in the disadvantages that are seen by HF models. These disadvantages are the large amount of computations resources and time it takes to run. This is typically due to the complexity of physics being calculated and is also impacted by the details of the mesh as well. Very detailed meshes requiring many nodes and elements thus increasing the simulation time. This simulation time is reduced used LF models or in this case Simple Structural Beam (SSB) model developed and presented in [9], [12], [74], [75], [76], [118].

This SSB model looks at representing the complex physical model as a system of beams. Doing so in this method eliminates the complex mesh analysis and physics and simplifies it, now is it possible to look as this from a modal analysis perspective using simple beams. The goal of a modal analysis is to fine the natural frequency of the system and its modal shapes. The process for finding the natural frequencies starts by looking at the global equation of motion Equation (3.21) and setting the force function *F(t)* equal to 0 as in Equation (3.22) the case of undamped free vibration [85]. In these equations d and $\ddot{d}$ represent the displacement and acceleration vectors, while K and M represent the global mass and stiffness matrices.

$$\{F(t)\} = [K]\{d\} + [M]\{\ddot{d}\} \tag{3.21}$$

$$[M]\{\ddot{d}\} + [K]\{d\} = 0 \tag{3.22}$$

The global mass and stiffness matrices define the motion of the structure and without any forces applied it becomes a second-order differential equation consisting of mass, stiffness, and displacement. The global matrices consider the geometric and material properties of the beams and are developed through the concatenated summation of the local matrices in Equation (3.23) and Equation (3.24).

$$[K] = \sum_{e=1}^{N} \left[k^{(e)}\right] \tag{3.23}$$

$$[M] = \sum_{e=1}^{N} \left[m^{(e)}\right] \tag{3.24}$$

To get the global matrices using SSB a structure is made up of beams represented by elements *p* connected to each other via nodes *n*. A beam is made up of 2 nodes connected by an element, where a node can be made up of 3 translational and 3 rotational making up a total of 6 degrees of freedom (DOF) thus when connected to another node via an element there are 12 DOF total. These beams by solving the local stiffness $k^{(e)}$ and mass $m^{(e)}$ matrices and subbing them into Equation (3.23) and Equation (3.24), can create the global stiffness matrix K^e and mass matrix M^e which can be seen in Equation (3.25) and Equation (3.26).

$$K^e = \begin{bmatrix}
\frac{AE}{L} & 0 & 0 & 0 & 0 & 0 & -\frac{AE}{L} & 0 & 0 & 0 & 0 & 0 \\
0 & \frac{12EI_z}{L^3} & 0 & 0 & 0 & \frac{6EI_z}{L^2} & 0 & -\frac{12EI_z}{L^3} & 0 & 0 & 0 & \frac{6EI_z}{L^2} \\
0 & 0 & \frac{12EI_y}{L^3} & 0 & -\frac{6EI_y}{L^2} & 0 & 0 & 0 & -\frac{12EI_y}{L^3} & 0 & -\frac{6EI_y}{L^2} & 0 \\
0 & 0 & 0 & \frac{GJ}{L} & 0 & 0 & 0 & 0 & 0 & -\frac{GJ}{L} & 0 & 0 \\
0 & 0 & -\frac{6EI_y}{L^2} & 0 & \frac{4EI_y}{L} & 0 & 0 & 0 & \frac{6EI_y}{L^2} & 0 & \frac{2EI_y}{L} & 0 \\
0 & \frac{6EI_z}{L^2} & 0 & 0 & 0 & \frac{4EI_z}{L} & 0 & -\frac{6EI_z}{L^2} & 0 & 0 & 0 & \frac{2EI_z}{L} \\
-\frac{AE}{L} & 0 & 0 & 0 & 0 & 0 & \frac{AE}{L} & 0 & 0 & 0 & 0 & 0 \\
0 & -\frac{12EI_z}{L^3} & 0 & 0 & 0 & -\frac{6EI_z}{L^2} & 0 & \frac{12EI_z}{L^3} & 0 & 0 & 0 & -\frac{6EI_z}{L^2} \\
0 & 0 & -\frac{12EI_y}{L^3} & 0 & \frac{6EI_y}{L^2} & 0 & 0 & 0 & \frac{12EI_y}{L^3} & 0 & \frac{6EI_y}{L^2} & 0 \\
0 & 0 & 0 & -\frac{GJ}{L} & 0 & 0 & 0 & 0 & 0 & \frac{GJ}{L} & 0 & 0 \\
0 & 0 & -\frac{6EI_y}{L^2} & 0 & \frac{2EI_y}{L} & 0 & 0 & 0 & \frac{6EI_y}{L^2} & 0 & \frac{4EI_y}{L} & 0 \\
0 & \frac{6EI_z}{L^2} & 0 & 0 & 0 & \frac{2EI_z}{L} & 0 & -\frac{6EI_z}{L^2} & 0 & 0 & 0 & \frac{4EI_z}{L}
\end{bmatrix} \tag{3.25}$$

$$M^e = \begin{bmatrix} \frac{1}{3} & 0 & 0 & 0 & 0 & 0 & \frac{1}{6} & 0 & 0 & 0 & 0 & 0 \\ 0 & \frac{13}{35} & 0 & 0 & 0 & \frac{11L}{210} & 0 & \frac{9}{70} & 0 & 0 & 0 & -\frac{13L}{420} \\ 0 & 0 & \frac{13}{35} & 0 & -\frac{11L}{210} & 0 & 0 & 0 & \frac{9}{70} & 0 & \frac{13L}{420} & 0 \\ 0 & 0 & 0 & \frac{I_y + I_z}{3A} & 0 & 0 & 0 & 0 & 0 & \frac{I_y + I_z}{6A} & 0 & 0 \\ 0 & 0 & -\frac{11L}{210} & 0 & \frac{L^2}{105} & 0 & 0 & 0 & -\frac{13L}{420} & 0 & -\frac{L^2}{140} & 0 \\ 0 & \frac{11L}{210} & 0 & 0 & 0 & \frac{L^2}{105} & 0 & \frac{13L}{420} & 0 & 0 & 0 & -\frac{L^2}{140} \\ \frac{1}{6} & 0 & 0 & 0 & 0 & 0 & \frac{1}{3} & 0 & 0 & 0 & 0 & 0 \\ 0 & \frac{9}{70} & 0 & 0 & 0 & \frac{13L}{420} & 0 & \frac{13}{35} & 0 & 0 & 0 & -\frac{11L}{210} \\ 0 & 0 & \frac{9}{70} & 0 & -\frac{13L}{420} & 0 & 0 & 0 & \frac{13}{35} & 0 & \frac{11L}{210} & 0 \\ 0 & 0 & 0 & \frac{I_y + I_z}{6A} & 0 & 0 & 0 & 0 & 0 & \frac{I_y + I_z}{3A} & 0 & 0 \\ 0 & 0 & \frac{13L}{420} & 0 & -\frac{L^2}{140} & 0 & 0 & 0 & \frac{11L}{210} & 0 & \frac{L^2}{105} & 0 \\ 0 & -\frac{13L}{420} & 0 & 0 & 0 & -\frac{L^2}{140} & 0 & -\frac{11L}{210} & 0 & 0 & 0 & \frac{L^2}{105} \end{bmatrix} \quad (3.26)$$

These global matrices represent geometric properties like cross sectional area of the beam *A,* the moments of inertia in the y axis I_y and z axis I_z, the polar moment of inertia *J* and the length *L*. In addition the material properties are incorporated as young's modulus *E*, shear modulus *G*, and density ρ [85]. The matrices define the motion of the structure that without any forces applied it becomes a second-order differential equation consisting of mass, stiffness, and displacement.

Once the global matrices are assembled it is now possible to take Equation (3.21) and solve it to procure the following Equation (3.27) where ω is the natural frequency vector. This can further be used to solve for the eigen values and vectors which will be the natural frequencies and mode shapes respectively.

$$|[K] - \omega^2[M]| = 0 \quad (3.27)$$

Now the LF model can be generated by defining the nodes and elements that correspond with the HF and physical model of the system. Therefore, by defining a start and end node an element beam can be identified. These elements are taken to be circular with a radius measured in meters. In addition, their parameters such as young's modulus, shear modulus, poisons ratio, and density can be defined here as well. The boundary conditions must also be set so that the proper matrices are formed, setting each of the 6 degrees of freedom for

each node as 1 to represent free or 0 to represent fixed. Creating the current physical twin setup leads to the creation of Figure 3-30 where each of the elements in black are separated by nodes in red.

When formulating the nodes and elements some consideration is taken is the division of the nodes and elements for this model. Like HF in that the finer the mesh the more accurate the results the more elements a component is made of in LF the greater in accuracy. Therefore, over the course of the beams that represent the shaft the shaft is split into a set number of elements due to the simplicity, in this case the program was set to split the beams into 4 equal parts. Since a large focus of this study is completed at the bearings it was important to make sure that the area that represents the bearing was split into numerous smaller beams to allow for more refinement on the properties and higher accuracy at those points. In this case it is possible to modify the parameters associated with an element of a very small area that represents the bearing without impacting large portions of the shaft. Finally, the fly wheel is created by defining several points on the radius and number of subdivisions like the shafts. In this case 5 points were taken for the radius making a pentagon, more points can be added slowly making the model trend closer to that of a circle but also increase computation resources, thus 5 was deemed sufficient to capture the shape of the flywheel with 4 divisions like the beams. Finally, at the location of the motor there is one extended vertical node, and at the bearings there is a horizontal and vertical extended node, these act as spring elements instead of beam elements. The purpose of the spring elements is to be able to modify the stiffness parameter on them to impact the system. With regards to the BDI having springs that impact stiffness and in the HF model where k_{11} and k_{22} bearing stiffness can be modified, the k_{11} and k_{22} bearings stiffness in LF are represented by these elements. Instead of the characteristics of the beams like density and young modulus the only parameter is the stiffness in N/m.

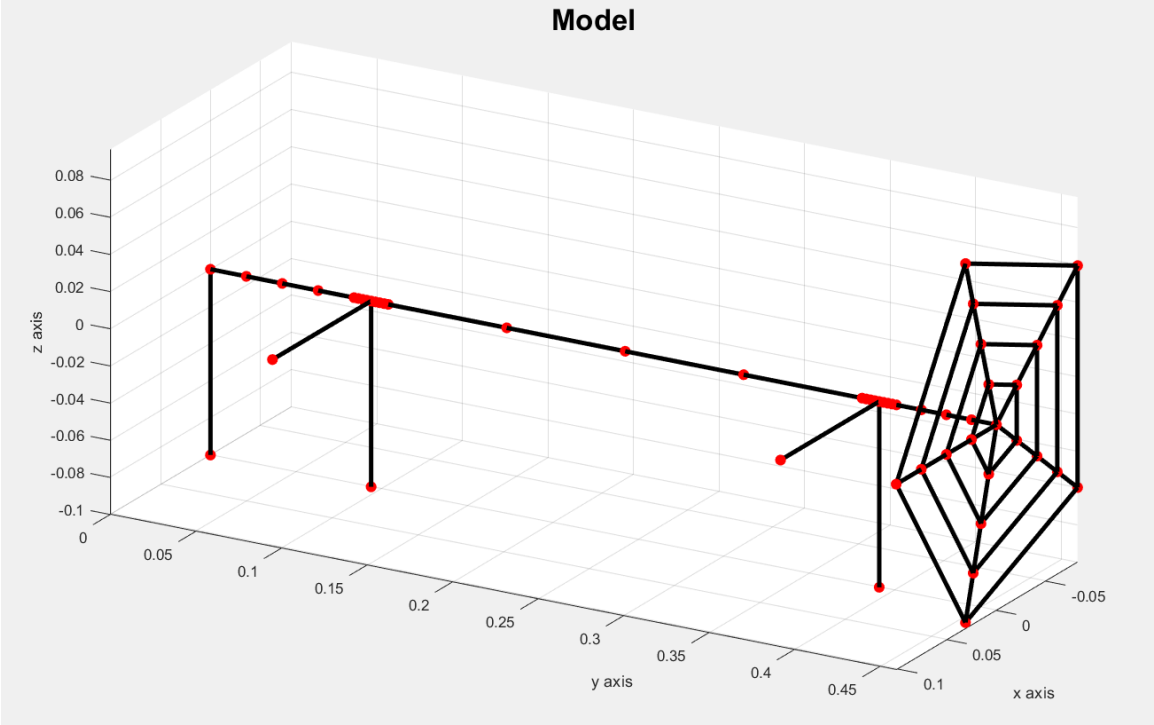

Figure 3-30: LF Model Made of Elements and Nodes

Chapter 4. Results

In this section the calibration of the LF and Hf models will be looked at to achieve the final versions for the DT. Then it will look at the resulting failure data that can be generated from those models and how they can be used to make a defect map that the physical twin can be compared to. This will then allow for the process of detecting if maintenance needs to be performed on the system or if it can continue operation. A flow chart of the optimization process can be seen below where the HF model is first solved to match the with physical twin before cycling back and repeating the process for the LF model modifying parameters as needed to reach desired results.

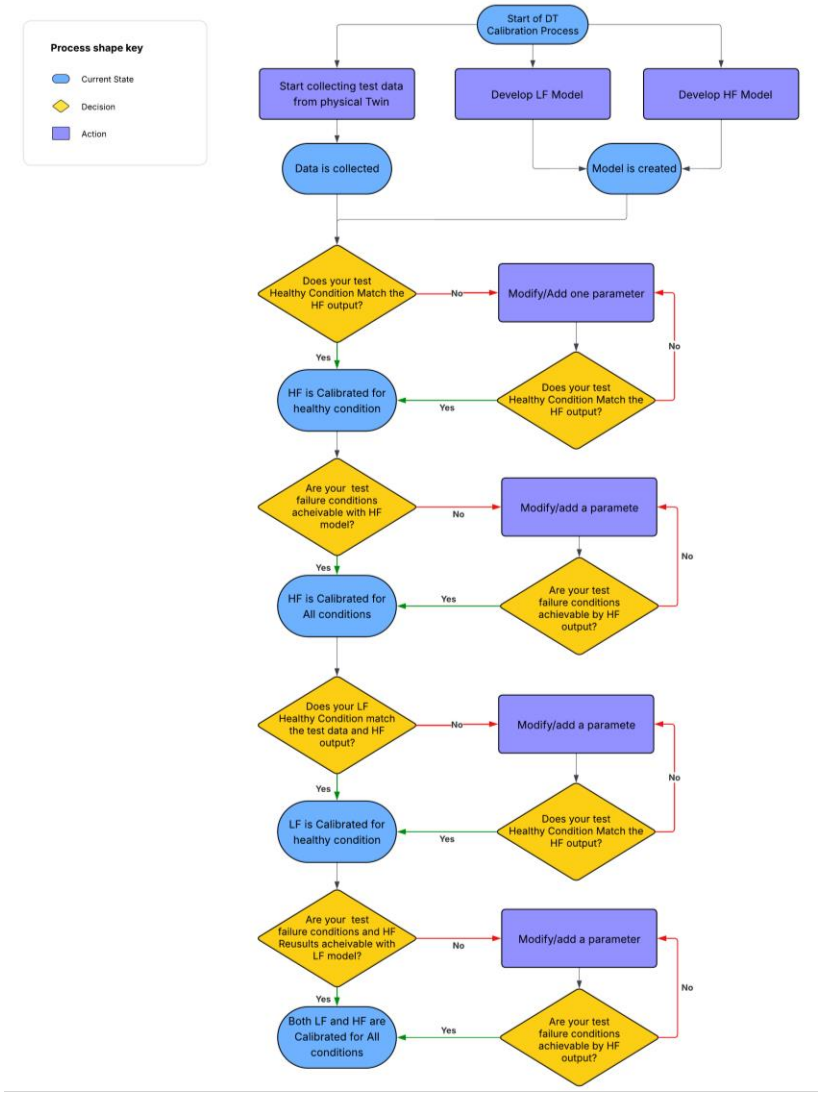

Figure 4-1: DT Calibration Flow Chart

4.1 High-Fidelity Optimization

The first step was the calibration of the HF twin with the physical twin before moving onto the LF twin. As mentioned previously in the methodology section it described the various components and that could be modified to change the results of the HF. It was initially started with the HF model matching all the material characteristics and having the properties in terms of weight matched as well. Then the positioning of all the features was set like Figure 3-28 but not completely the same as that image shows the final HF model. Next an arbitrary value of 50000 N/m or 50 N/mm was selected as the stiffness of the bearings in healthy condition based on the closeness to some of the tested values from the BDI and spring tests. Upon running the first simulation, it was seen that there was a first natural frequency of about 66Hz which was much higher than expected. To compensate for this large difference changes to the model were made to have the solid shaft turned into a keyed shaft which would slightly reduce the rigidity of the shaft and make it more accurate. The second change was in the distance of the fixed end, initially the fixed end was designated at the middle of the shaft collar directly before the bearing, to add less rigidity it was extended by 4in to line up to the centre of the motor mass, resulting in a much lower frequency of 26.19Hz in Figure 4-2. Considering the large effect that the length had on the system the length of that fixed support was changed to the beginning of where the motor bearing is before turning into the case of the motor, about 3.7in away from the support bearing as seen in Figure 3-28 resulting in a 31.55Hz which is slightly higher than the test setup.

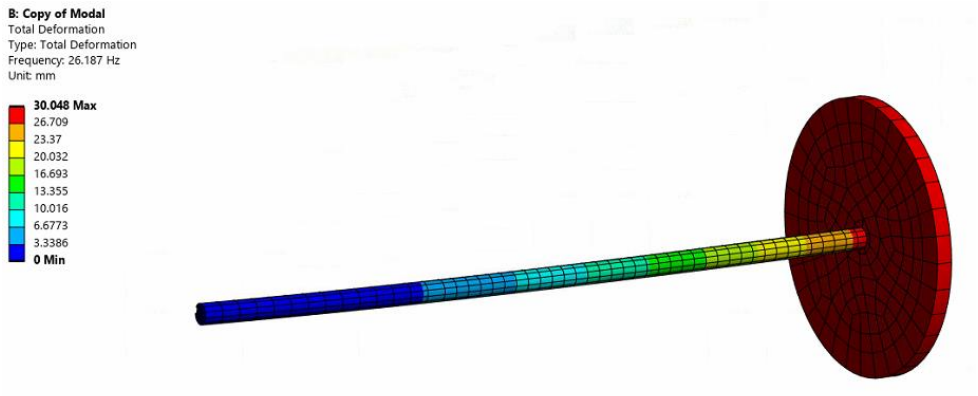

Figure 4-2: HF Model with Elongated Shaft

Continuing from this point the next area that was focused on to modify the frequency output was the stiffness of the bearings. Using batch simulating it was possible to run through many potential stiffness values ranging from 0.1 N/mm up to 50 N/mm as mentioned earlier. It was eventually narrowed down to 31 N/m that results in an output frequency of 27.551 Hz matching very closely to the results of the BDI testing in a healthy condition. The mode shapes of the system were found to be consistent and not relevant to the results and only the first natural frequency was found necessary at this time.

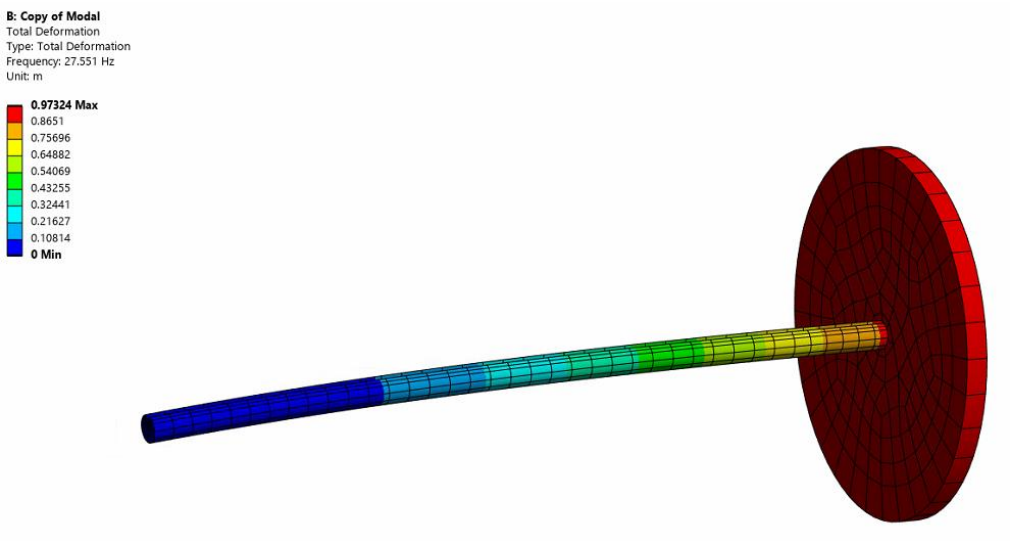

Figure 4-3: Calibrated HF Model for Healthy Condition

Once the healthy condition was established and calibrated for the next step was to also calibrate for the unhealthy conditions. As mentioned, prior when considering the data and inconsistencies earlier it was determined that an important factor in the changes of frequency was a result of the BDI. When only modifying the BDI bearing stiffness to represent the drop in health of the bearing the following stiffnesses and the resulting frequencies were determined Table 4-1. What is clear from this table is that when compared to Table 3-6 the lower end of the frequencies is not attainable simply by stiffness modulation alone. Therefore, to incorporate the lower frequencies an additional change to the HF model must be made. Previously it was mentioned how through the nature of how the BDI works there would be an impact from the hanging mass because of being suspended by springs. Thus, when the BDI is in a state of reduced health/stiffness more weight is impacted onto the shaft due to the hanging mass of the bearing and the base plate

of which it sits. This added mass creates shifts in the frequency lower as the system experiences more disturbances because of this added weight.

Table 4-1: Simulated Bearing Stiffness and Resulting Peak Natural Frequencies

Simulated Bearing Stiffness (N/mm)	Simulated Peak Frequency (Hz)
35	28.447
31	27.551
30	27.327
25	26.154
20	24.919
15	23.613
10	22.223
5	20.733
0.1	19.453

To account for the added weight of the hanging bearing and base plate a point mass is added at the point of the BDI bearing. This mass was modified to account for the hanging mass seen in the actual test results. To determine what the range of masses will be needed to represent all the health conditions another batch simulation was completed that cycled through a range of masses from 0 to 5kg with every combination of the bearing stiffness resulting in the simulation of 2601 data points. From the results several combinations resulted in the formulation of a peak frequency like that of the lowest tested frequency, the one with the lowest added mass value was chosen with the total combination being an added mass of 3.4 kg, BDI bearing stiffness of 0.1 N/m. The resulting modal shape and frequency can be seen in Figure 4-4. Now all the frequency values from the physical twin's test can be represented by a combination of bearing stiffness between 0.1 N/m to 31 N/m and an added moving mass value of 0 kg to 3.4 kg.

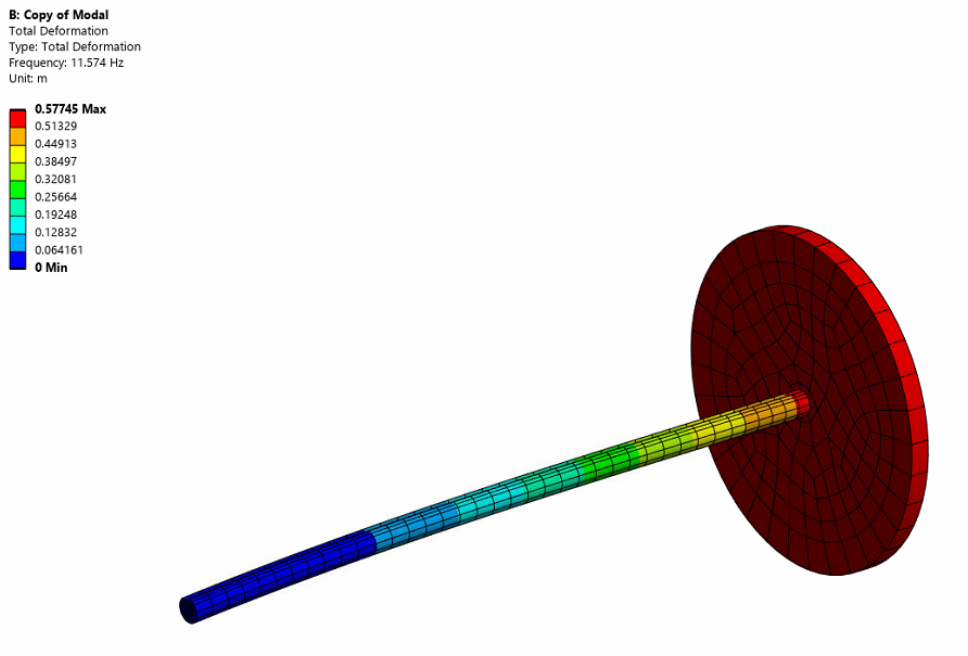

Figure 4-4: HF Simulation for Lowest Health Condition Achieved

4.2 Low-Fidelity Optimization

Once the HF model is complete it is now time to optimize the low fidelity model. The goal is to again generate results using the LF that closely matches the physical twins' results but also match the HF results so that the test data, high fidelity, and low fidelity all match. As mentioned in the methodology section one of the edits made to the model to improve it was the additional beam segments at the location of the bearings for increase fidelity. After the modification to the beams at the bearings the LF framework was complete, and the model was ready for calibration with healthy condition. Since the LF model is a simplified version of the HF when looking at the first parameter to modify, the stiffness of the bearing elements was the first to try. Thus, from the HF simulations the stiffness values for the bearings were set at 31 N/m which resulted in a frequency very similar to that of the HF and physical twin Figure 4-5, thus no changes were needed for the healthy condition other than matching the stiffness.

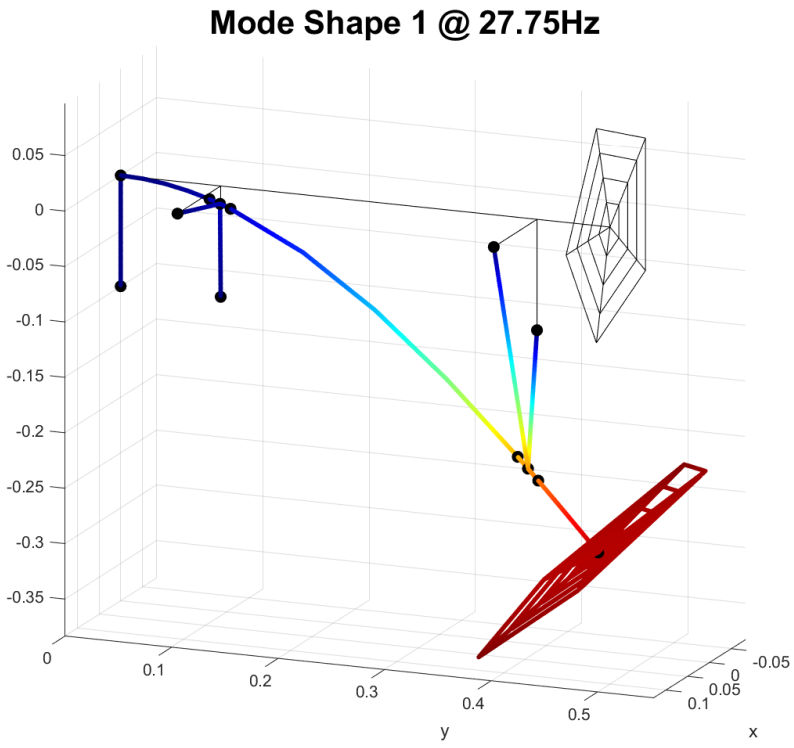

Figure 4-5: Healthy BDI Bearing Frequency in LF

Next was the calibration of the LF for the unhealthy cases which like the HF did not match the physical twin results simply by decreasing the stiffness. The next addition to calibrate the LF was the creation of a health factor that represent the health of the system from 0 to 100. This was simply done by implementing the following Equation (4.1) where k_b is the variable bearing stiffness and hf is the health factor variable ranging from 0 to 1.

$$k_b = (31000)\ (\text{hf}) \tag{4.1}$$

In addition, through HF it was determined that an added mass was needed at the test bearing location to account for impact the BDI has on the system in low health/stiffness conditions. To account for this impact, it was important to consider the relationship between the added mass on the shaft to the health of the bearing from the BDI. As the health of the bearing is lowered by the BDI the mass impact on the shaft is increased. Therefore, one method to achieve this is to increase the mass of the beam representing the BDI by modifying the density. In doing this it is also important to understand the relation between the floating moving mass and the stiffness of the system. Thus, the following formula was used to define density as a relation of a health factor ranging from 0 (Unhealthy) to 1 (Healthy) and a Mass Factor ranging from 0 (Unhealthy or full added moving mass effect) to 1

(Healthy or no added moving mass effect). The formula is designed in a way so that when the health factor is a value of 1 (100% Healthy) then the right side of the equation becomes 0 meaning there is no impact on the density value of 7850 GP and no change is made giving the same results that were seen in the healthy calibration. In the case where hf is not 1 then the rest of the right side will have impact where if mf is 1 then there is no mass impact so the right side becomes 0 again but otherwise it will affect the density. Finally, the value of 130 is a constant that was achieved through batch simulation to find what value will give the lowest frequency value seen in our physical testing like what was done with the added mass during HF calibration. Now that the LF is calibrated a batch sim can be completed to generate a 2D map of failure data with respect to the health and mass factor in figure

$$\rho = 7850\big(1 + 130(1 - hf)(1 - mf)\big) \tag{4.2}$$

Now that the LF is calibrated a batch sim can be completed to generate a 2D map of failure data with respect to the health and mass factor in relation to frequency as seen in Figure 4-6. This map can be used as a check for the health of the system, where if the frequency lands in the green area it can be considered healthy while the other areas are for damaged and failed bearing.

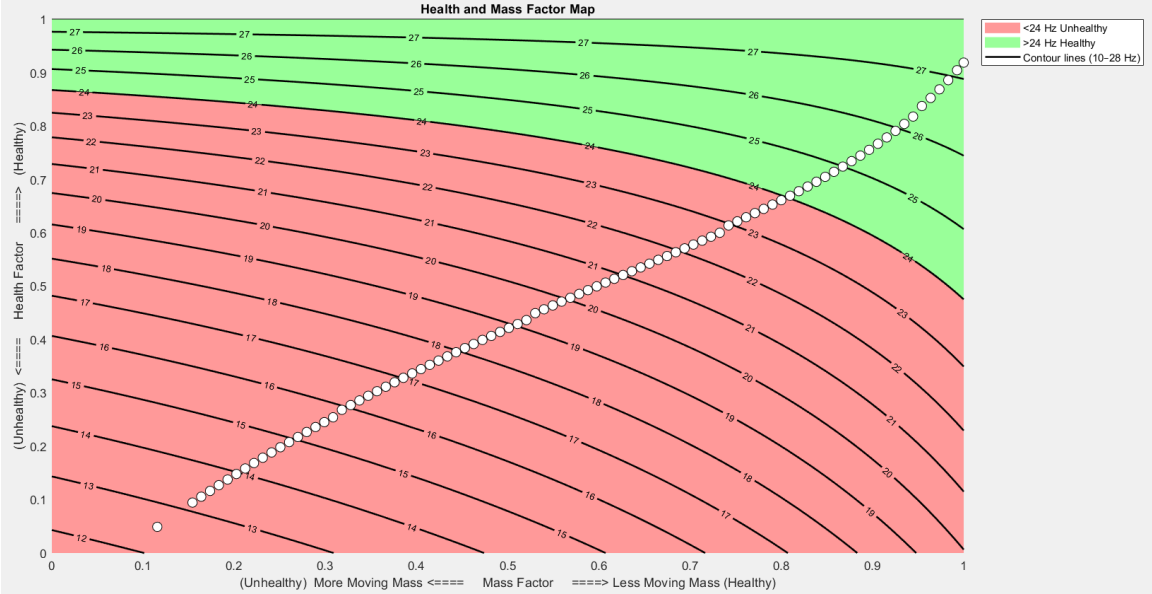

Figure 4-6: 2D Map of Relation Between Health Factor, Mass Factor, and Frequency

4.3 System Health Analysis and Maintenance Planning

The health of the system can now be found using the LF 2D map in Figure 4-6 with a flow chart of this process shown in Figure 4-7.

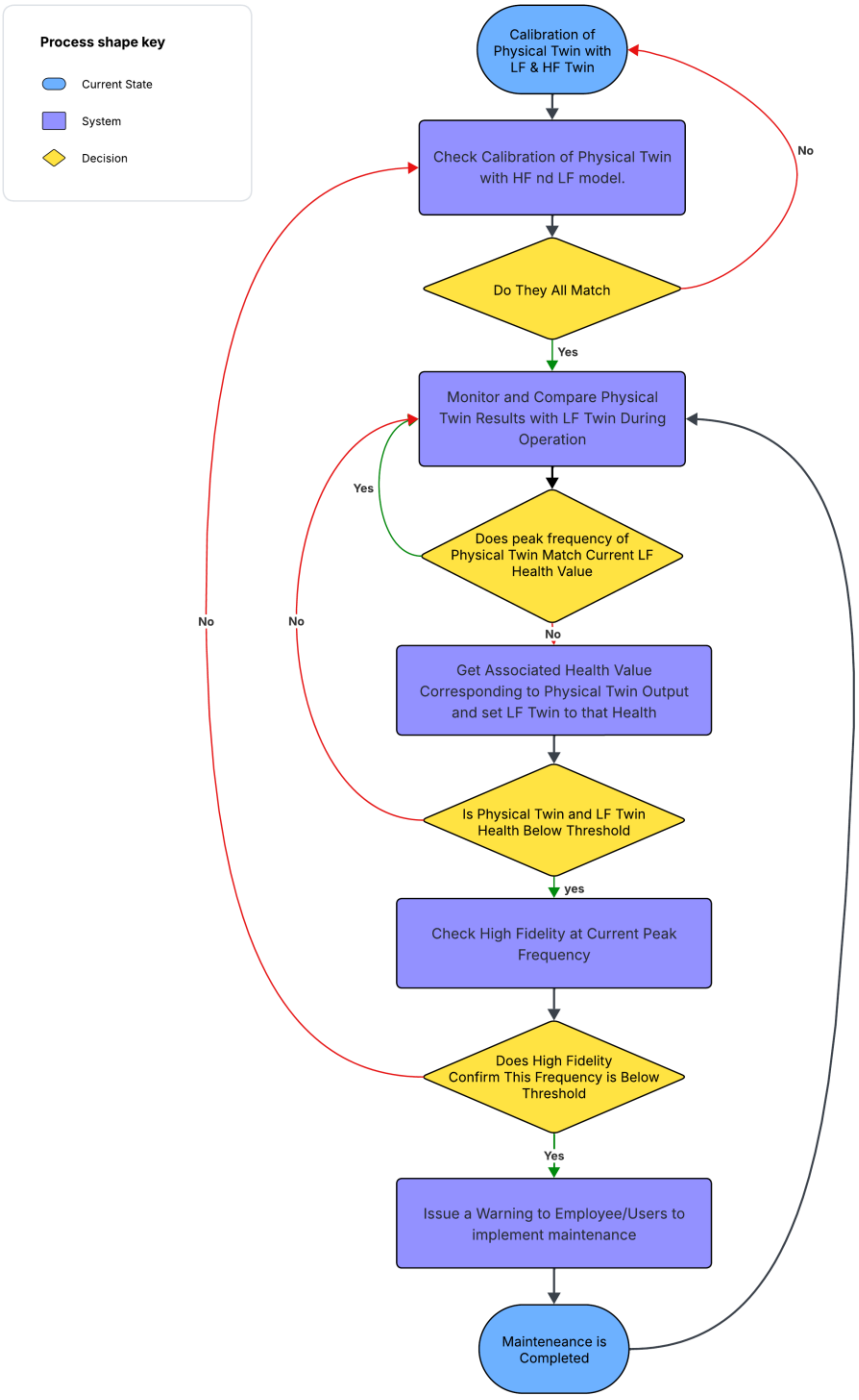

Figure 4-7: Flow Chart for DT System Health Check

For example, the results of a test from the physical twin will give an output in the form of a peak frequency. Therefore, by rewriting the line of best fit equation from Figure 3-27 the health factor can be found from Equation (4.3) by isolating for the y to get the stiffness, and then dividing by the max stiffness to place the health factor on a scale from 0 to 1. Now with the frequency and the health factor these can be used to find the mass factor on the 2D map placing the result in one of the zones. This can then be used as a check to determine if the system is healthy and if maintenance should be performed.

$$hf = \left(\frac{f - 10.16}{0.6403}\right)\left(\frac{1}{25.94}\right) \tag{4.3}$$

An example of how the 2D map works can be demonstrated by performing the calculation for several points and then plotting them in the map and extrapolating the mass factor from it. This was done and the result is shown in Figure 4-8 with the data points shown, and areas grayed out. Now it is important to consider that this line is an estimated line of best fit so there can be some deviations and in accuracies thus an estimated band can be created slightly above and below this line to account for any of the inaccuracies. This also makes sense from a logical standpoint because if you look at the upper left grayed out triangle the top left point would have a health factor of 1 and a mass factor of 0. When considering the test setup there is no case where there is a lot of moving mass impacting the system while having perfect stiffness so this area can be disregarded. Additionally, the same can be said for the bottom right area where there is not a case where the stiffness factor will be 0 meaning a very loose system, thus there would not be many if any moving mass. Therefore, from a logical standpoint of the system it makes sense to disregard these areas.

Once it is confirmed that from the LF simulation that it is a potential failed bearing and requires maintenance the HF model will also be checked in a similar method to confirm that this frequency is a call for maintenance. Thus, this will complete the DT cycle of monitoring the system and confirming the health for the user. The system is resistant to false alarms as the system has access to historical data in addition to continuously running every few seconds allowing it for many checks that the alarm is represented of the actual condition.

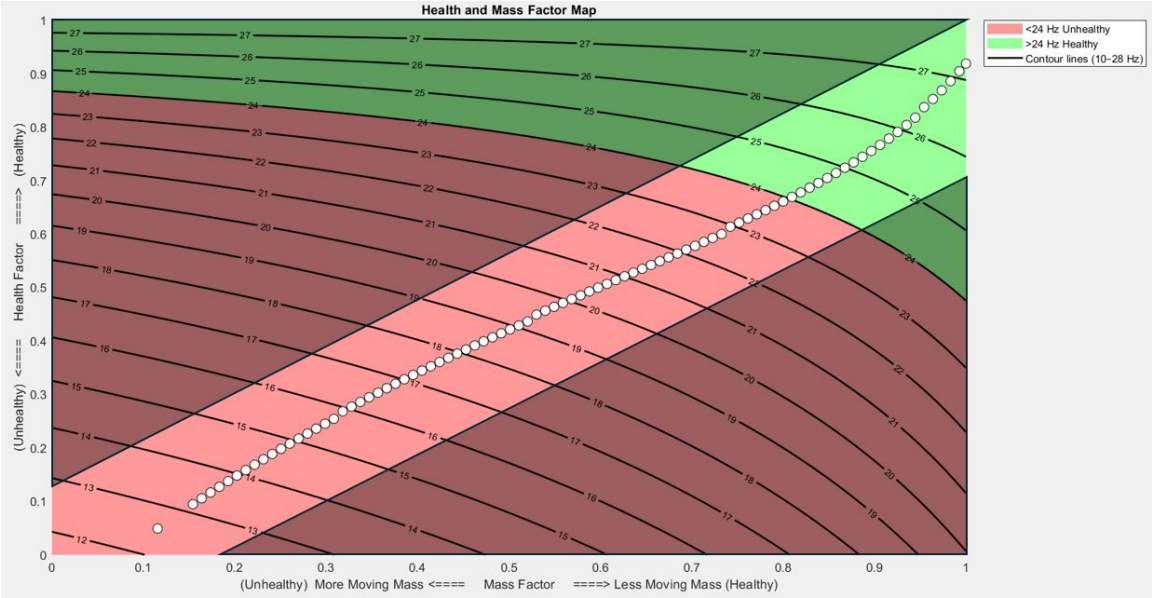

Figure 4-8: 2D Map of Relation Between Health Factor, Mass Factor, and Frequency with Grayed out section and Estimated line of values.

4.4 Simulation Resources

One of the concerns mentioned with DTs and simulations in general is the number of resources they take. The benefit of the LIVE DT System is the creation of an LF model that replaces a large amount of the work HF simulations would need to do, thus reducing time and resources needed. LF does not require a significant amount of time and resources when compared to the HF model. This can be demonstrated through the simulation times in this research and represented on a graph using a logarithmic scale. Samples were taken from each of the simulations and the simulation time was averaged out for each one. The average times were then extrapolated to give the result in Figure 4-9. From this it is seen that projected for 10000 simulations it would take about 20 minutes for the LF but over 50 hours for the HF simulation making HF 150 times longer to complete 10000 simulations. It is important to consider this simulation are for a very simple system, thus the difference could be even more significant in more complex systems with many more components and detailed meshes.

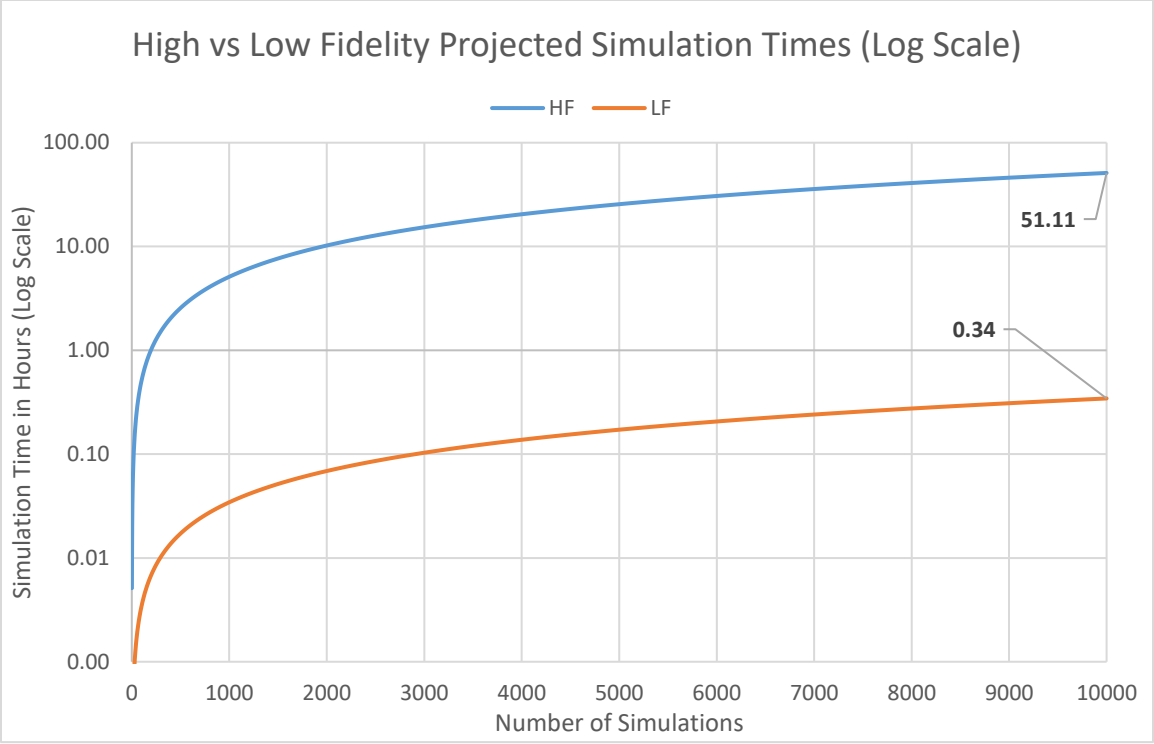

Figure 4-9: LF Vs High Fidelity Simulation Time

Chapter 5. Conclusions

In the objectives section the main goals of this thesis were stated. These goals consisted of the demonstration of the LIVE Digital Twin methodology for bearings in dynamic rotary systems. In this thesis the LIVE DT method was applied to an induction motor successfully covering the use of dynamic systems. In addition, the LIVE DT method was shown to complete the calibration between the 3 entities of the physical twin, LF twin, and HF twin making LIVE Triplets to reach the same conclusions on the health of a rotary system. Additional objectives of this thesis included the ability to reliably and repeatedly generate failure data for defined levels of damage to a bearing to greatly reduce the testing period of working system. It was also important to consider the reduction of simulation time and resources that the LIVE process encourages and enables.

This thesis was to apply the LIVE DT to a rotary machinery system to be able to calibrate the 3 entities between the physical twin, high fidelity model and low fidelity model. In this work all three of the entities were calibrated to each other by the end of the research allowing for the prediction of health of all 3 systems. The additional objectives of being able to develop failure data consistently was also achieved through innovative research in the bearing defect inducer (BDI). The results from the BDI were useful in being able to generate failure data and calibrate the HF and LF models proving the advantages of being able to manually generate failure data for a DT system. This is expressed while also showing how this process can reduce the cost of simulation in similar maintenance strategies due to the LIVE methodology. Thus, this thesis thoroughly succeeds in showcasing the design and development of the LIVE DT Methodology for predictive maintenance in rotary machinery Systems by being able to receive the artificially created failure data from the physical dynamic system, run it through the calibrated digital models and predict failure of the system and recommend maintenance to the user.

5.1 Future Work

This thesis like any work has many areas in which it can be further improved and explored for future work. One such opening for improvement and future work is the other renditions of the BDI described in the thesis. Some of these BDI designs are unique designs that could

be applied to other scenarios in which failure data may be generated. Some additional time into the study and manufacturing of these items can lead to additional improvements and methods of developing failure data. An additional, potential area for improvement is the expansion of the rotary machinery system. In this thesis it shows an earlier design of the rotary machine system with many additional elements in the system. Future work incorporating some of those additional features would allow for and even more in-depth study on rotary machinery in addition to also confirm the ability of the LIVE DT methodology for more complex systems. Another key area of improvement would be applying what was accomplished in this thesis to work in a real time scenario. Although the objectives of this thesis are only on the design and calibration it could be very innovative and useful work to continue the LIVE DT process and apply this system in real time. In addition, the use of ML and AI can be implemented to help enhance the predictive maintenance capabilities of the healthy prediction system.

References

[1] H. Gohari, A. Barari, H. Kishawy, and M. S. G. Tsuzuki, “Intelligent Process Planning for Additive Manufacturing,” *IFAC-Pap.*, vol. 52, no. 10, pp. 218–223, 2019, doi: 10.1016/j.ifacol.2019.10.067.

[2] C. Berry and A. Barari, “Cyber-Physical System Utilizing Work-Piece Memory in Digital Manufacturing,” *IFAC-Pap.*, vol. 52, no. 10, pp. 201–206, Jan. 2019, doi: 10.1016/j.ifacol.2019.10.023.

[3] Q. Qi, D. Zhao, T. W. Liao, and F. Tao, “Modeling of Cyber-Physical Systems and Digital Twin Based on Edge Computing, Fog Computing and Cloud Computing Towards Smart Manufacturing,” in *Volume 1: Additive Manufacturing; Bio and Sustainable Manufacturing*, College Station, Texas, USA: American Society of Mechanical Engineers, June 2018, p. V001T05A018. doi: 10.1115/MSEC2018-6435.

[4] M. Bärring, B. Johansson, and G. Shao, “Digital Twin for Smart Manufacturing: The Practitioner’s Perspective,” in *Volume 2B: Advanced Manufacturing*, Virtual, Online: American Society of Mechanical Engineers, Nov. 2020, p. V02BT02A015. doi: 10.1115/IMECE2020-24037.

[5] M. G. Juarez, V. J. Botti, and A. S. Giret, “Digital Twins: Review and Challenges,” *J. Comput. Inf. Sci. Eng.*, vol. 21, no. 3, p. 030802, June 2021, doi: 10.1115/1.4050244.

[6] E. Gülbahçe and M. Çelik, “Experimental modal analysis for the plate structures with roving inertial shaker method approach,” *J. Low Freq. Noise Vib. Act. Control*, vol. 41, no. 1, pp. 27–40, Mar. 2022, doi: 10.1177/14613484211039323.

[7] H. Askari, E. Esmailzadeh, and A. Barari, “A unified approach for nonlinear vibration analysis of curved structures using non-uniform rational B-spline representation,” *J. Sound Vib.*, vol. 353, pp. 292–307, Sept. 2015, doi: 10.1016/j.jsv.2015.05.022.

[8] Ö. E. Genel, M. Tüfekci, and E. Tüfekci, “Free vibrations of spatial frame structures: Analytical modelling and solution,” *J. Vib. Control*, vol. 29, no. 19–20, pp. 4492–4502, Oct. 2023, doi: 10.1177/10775463221122086.

[9] N. G. Malek, M. Tayefeh, D. Bender, and A. Barari, “LIVE Digital Twin for Smart Maintenance in Structural Systems,” *IFAC-Pap.*, vol. 54, no. 1, pp. 1047–1052, Jan. 2021, doi: 10.1016/j.ifacol.2021.08.124.

[10] F. Tao, H. Zhang, A. Liu, and A. Y. C. Nee, “Digital Twin in Industry: State-of-the-Art,” *IEEE Trans. Ind. Inform.*, vol. 15, no. 4, pp. 2405–2415, Apr. 2019, doi: 10.1109/TII.2018.2873186.

[11] J. Wang, L. Ye, R. X. Gao, C. Li, and L. Zhang, “Digital Twin for rotating machinery fault diagnosis in smart manufacturing,” *Int. J. Prod. Res.*, vol. 57, no. 12, pp. 3920–3934, June 2019, doi: 10.1080/00207543.2018.1552032.

[12] A. E. Bondoc, “Developing a Calibrated Low Fidelity Model and an Optimized Sensor Network Using LIVE Digital Twin for Pipelines in Oil and Gas Industries”.

[13] Y. E. Karabacak and N. Gürsel Özmen, “Common spatial pattern-based feature extraction and worm gear fault detection through vibration and acoustic measurements,” *Measurement*, vol. 187, p. 110366, Jan. 2022, doi: 10.1016/j.measurement.2021.110366.

[14] A. E. Bondoc *et al.*, “Implementation of LIVE Digital Twin Enabled Smart Maintenance Using Smart Structural Sensors,” in *2023 15th IEEE International*

Conference on Industry Applications (INDUSCON), São Bernardo do Campo, Brazil: IEEE, Nov. 2023, pp. 1205–1212. doi: 10.1109/INDUSCON58041.2023.10374903.
[15] Z. Peng and N. Kessissoglou, "An integrated approach to fault diagnosis of machinery using wear debris and vibration analysis," *Wear*, vol. 255, no. 7–12, pp. 1221–1232, Aug. 2003, doi: 10.1016/S0043-1648(03)00098-X.
[16] K. Y. H. Lim, P. Zheng, C.-H. Chen, and L. Huang, "A digital twin-enhanced system for engineering product family design and optimization," *J. Manuf. Syst.*, vol. 57, pp. 82–93, Oct. 2020, doi: 10.1016/j.jmsy.2020.08.011.
[17] W. Luo, T. Hu, Y. Ye, C. Zhang, and Y. Wei, "A hybrid predictive maintenance approach for CNC machine tool driven by Digital Twin," *Robot. Comput.-Integr. Manuf.*, vol. 65, p. 101974, Oct. 2020, doi: 10.1016/j.rcim.2020.101974.
[18] C. Berry and A. Barari, "Closed-Loop Coordinate Metrology for Hybrid Manufacturing System," *IFAC-Pap.*, vol. 51, no. 11, pp. 752–757, 2018, doi: 10.1016/j.ifacol.2018.08.409.
[19] P. M. Djuric *et al.*, "Particle Filtering," *IEEE Signal Process. Mag.*, vol. 20, no. 5, pp. 19–38, Sept. 2003, doi: 10.1109/MSP.2003.1236770.
[20] F. Yang, R. Sedaghati, and E. Esmailzadeh, "Seismic Response Controlled Structure With Semi-Active Mass-Damper," in *Volume 5: Design, Analysis, Control and Diagnosis of Fluid Power Systems*, Boston, Massachusetts, USA: ASMEDC, Jan. 2008, pp. 169–175. doi: 10.1115/IMECE2008-69001.
[21] W. Kritzinger, M. Karner, G. Traar, J. Henjes, and W. Sihn, "Digital Twin in manufacturing: A categorical literature review and classification," *IFAC-Pap.*, vol. 51, no. 11, pp. 1016–1022, 2018, doi: 10.1016/j.ifacol.2018.08.474.
[22] F. Tao *et al.*, "Digital twin-driven product design framework," *Int. J. Prod. Res.*, vol. 57, no. 12, pp. 3935–3953, June 2019, doi: 10.1080/00207543.2018.1443229.
[23] F. Tao, J. Cheng, Q. Qi, M. Zhang, H. Zhang, and F. Sui, "Digital twin-driven product design, manufacturing and service with big data," *Int. J. Adv. Manuf. Technol.*, vol. 94, no. 9–12, pp. 3563–3576, Feb. 2018, doi: 10.1007/s00170-017-0233-1.
[24] S. Muralidharan, B. Yoo, and H. Ko, "Designing a Semantic Digital Twin model for IoT," in *2020 IEEE International Conference on Consumer Electronics (ICCE)*, Las Vegas, NV, USA: IEEE, Jan. 2020, pp. 1–2. doi: 10.1109/ICCE46568.2020.9043088.
[25] S. Bellis and J. Denil, "Challenges and possible approaches for sustainable digital twinning," in *Proceedings of the 25th International Conference on Model Driven Engineering Languages and Systems: Companion Proceedings*, Montreal Quebec Canada: ACM, Oct. 2022, pp. 643–648. doi: 10.1145/3550356.3561551.
[26] S. Malakuti, "Emerging Technical Debt in Digital Twin Systems," in *2021 26th IEEE International Conference on Emerging Technologies and Factory Automation (ETFA)*, Vasteras, Sweden: IEEE, Sept. 2021, pp. 01–04. doi: 10.1109/ETFA45728.2021.9613538.
[27] M. S. Gill, L.-T. Reiche, and A. Fay, "Method for selecting Digital Twins of Entities in a System-of-Systems approach based on essential Information Attributes," in *2022 IEEE 27th International Conference on Emerging Technologies and Factory Automation (ETFA)*, Stuttgart, Germany: IEEE, Sept. 2022, pp. 1–8. doi: 10.1109/ETFA52439.2022.9921489.

[28] Križanić, Snježana; Vrček, Neven, “Business process modeling and digital twins: a literature review,” in *Central European Conference on Information and Intelligent Systems*, Varazdin: Faculty of Organization and Informatics Varazdin, 2023, pp. 141–151.
[29] R. Van Dinter, B. Tekinerdogan, and C. Catal, “Predictive maintenance using digital twins: A systematic literature review,” *Inf. Softw. Technol.*, vol. 151, p. 107008, Nov. 2022, doi: 10.1016/j.infsof.2022.107008.
[30] M. Vathoopan, M. Johny, A. Zoitl, and A. Knoll, “Modular Fault Ascription and Corrective Maintenance Using a Digital Twin,” *IFAC-Pap.*, vol. 51, no. 11, pp. 1041–1046, 2018, doi: 10.1016/j.ifacol.2018.08.470.
[31] Y. Xu, Y. Sun, X. Liu, and Y. Zheng, “A Digital-Twin-Assisted Fault Diagnosis Using Deep Transfer Learning,” *IEEE Access*, vol. 7, pp. 19990–19999, 2019, doi: 10.1109/ACCESS.2018.2890566.
[32] P. Aivaliotis, K. Georgoulias, Z. Arkouli, and S. Makris, “Methodology for enabling Digital Twin using advanced physics-based modelling in predictive maintenance,” *Procedia CIRP*, vol. 81, pp. 417–422, 2019, doi: 10.1016/j.procir.2019.03.072.
[33] P. Aivaliotis, K. Georgoulias, and G. Chryssolouris, “The use of Digital Twin for predictive maintenance in manufacturing,” *Int. J. Comput. Integr. Manuf.*, vol. 32, no. 11, pp. 1067–1080, Nov. 2019, doi: 10.1080/0951192X.2019.1686173.
[34] H. Ding, L. Yang, and Z. Yang, “A Predictive Maintenance Method for Shearer Key Parts Based on Qualitative and Quantitative Analysis of Monitoring Data,” *IEEE Access*, vol. 7, pp. 108684–108702, 2019, doi: 10.1109/ACCESS.2019.2933676.
[35] J. Lee, F. Wu, W. Zhao, M. Ghaffari, L. Liao, and D. Siegel, “Prognostics and health management design for rotary machinery systems—Reviews, methodology and applications,” *Mech. Syst. Signal Process.*, vol. 42, no. 1–2, pp. 314–334, Jan. 2014, doi: 10.1016/j.ymssp.2013.06.004.
[36] A. Faizan, “Electric Motor Failure Causes.” [Online]. Available: https://electricalacademia.com/motor-control/electric-motor-failure-causes/
[37] M. Wrzochal, “Comparative analysis of the structural solutions of bearing vibration test equipment used in quality control procedures,” *Int. J. Adv. Manuf. Technol.*, vol. 125, no. 9, pp. 4047–4063, Apr. 2023, doi: 10.1007/s00170-023-11029-5.
[38] J. F. D. Santos *et al.*, “Digital Twin-Based Monitoring System of Induction Motors Using IoT Sensors and Thermo-Magnetic Finite Element Analysis,” *IEEE Access*, vol. 11, pp. 1682–1693, 2023, doi: 10.1109/ACCESS.2022.3232063.
[39] S. S. Goundar, M. R. Pillai, K. A. Mamun, F. R. Islam, and R. Deo, “Real time condition monitoring system for industrial motors,” in *2015 2nd Asia-Pacific World Congress on Computer Science and Engineering (APWC on CSE)*, Nadi, Fiji: IEEE, Dec. 2015, pp. 1–9. doi: 10.1109/APWCCSE.2015.7476232.
[40] W. Hu, T. Wang, and F. Chu, “Novel Ramanujan Digital Twin for Motor Periodic Fault Monitoring and Detection,” *IEEE Trans. Ind. Inform.*, vol. 19, no. 12, pp. 11564–11572, Dec. 2023, doi: 10.1109/TII.2023.3248110.
[41] F. Tao, M. Zhang, Y. Liu, and A. Y. C. Nee, “Digital twin driven prognostics and health management for complex equipment,” *CIRP Ann.*, vol. 67, no. 1, pp. 169–172, 2018, doi: 10.1016/j.cirp.2018.04.055.

[42] A. Barthelmey, E. Lee, R. Hana, and J. Deuse, “Dynamic digital twin for predictive maintenance in flexible production systems,” in *IECON 2019 - 45th Annual Conference of the IEEE Industrial Electronics Society*, Lisbon, Portugal: IEEE, Oct. 2019, pp. 4209–4214. doi: 10.1109/IECON.2019.8927397.
[43] A. Werner, N. Zimmermann, and J. Lentes, “Approach for a Holistic Predictive Maintenance Strategy by Incorporating a Digital Twin,” *Procedia Manuf.*, vol. 39, pp. 1743–1751, 2019, doi: 10.1016/j.promfg.2020.01.265.
[44] S. Venkatesan, K. Manickavasagam, N. Tengenkai, and N. Vijayalakshmi, “Health monitoring and prognosis of electric vehicle motor using intelligent-digital twin,” *IET Electr. Power Appl.*, vol. 13, no. 9, pp. 1328–1335, Sept. 2019, doi: 10.1049/iet-epa.2018.5732.
[45] Z. Liu, W. Chen, C. Zhang, C. Yang, and H. Chu, “Data Super-Network Fault Prediction Model and Maintenance Strategy for Mechanical Product Based on Digital Twin,” *IEEE Access*, vol. 7, pp. 177284–177296, 2019, doi: 10.1109/ACCESS.2019.2957202.
[46] W. Luo, T. Hu, C. Zhang, and Y. Wei, “Digital twin for CNC machine tool: modeling and using strategy,” *J. Ambient Intell. Humaniz. Comput.*, vol. 10, no. 3, pp. 1129–1140, Mar. 2019, doi: 10.1007/s12652-018-0946-5.
[47] Q. Qiao, J. Wang, L. Ye, and R. X. Gao, “Digital Twin for Machining Tool Condition Prediction,” *Procedia CIRP*, vol. 81, pp. 1388–1393, 2019, doi: 10.1016/j.procir.2019.04.049.
[48] S. Centomo, N. Dall’Ora, and F. Fummi, “The Design of a Digital-Twin for Predictive Maintenance,” in *2020 25th IEEE International Conference on Emerging Technologies and Factory Automation (ETFA)*, Vienna, Austria: IEEE, Sept. 2020, pp. 1781–1788. doi: 10.1109/ETFA46521.2020.9212071.
[49] M. Xiong, H. Wang, Q. Fu, and Y. Xu, “Digital twin–driven aero-engine intelligent predictive maintenance,” *Int. J. Adv. Manuf. Technol.*, vol. 114, no. 11–12, pp. 3751–3761, June 2021, doi: 10.1007/s00170-021-06976-w.
[50] H. Huang, L. Yang, Y. Wang, X. Xu, and Y. Lu, “Digital Twin-driven online anomaly detection for an automation system based on edge intelligence,” *J. Manuf. Syst.*, vol. 59, pp. 138–150, Apr. 2021, doi: 10.1016/j.jmsy.2021.02.010.
[51] X. Yang, Y. Ran, G. Zhang, H. Wang, Z. Mu, and S. Zhi, “A digital twin-driven hybrid approach for the prediction of performance degradation in transmission unit of CNC machine tool,” *Robot. Comput.-Integr. Manuf.*, vol. 73, p. 102230, Feb. 2022, doi: 10.1016/j.rcim.2021.102230.
[52] F. Pires, A. Cachada, J. Barbosa, A. P. Moreira, and P. Leitão, “Digital Twin in Industry 4.0: Technologies, Applications and Challenges,” in *2019 IEEE 17th International Conference on Industrial Informatics (INDIN)*, Helsinki, Finland: IEEE, July 2019, pp. 721–726. doi: 10.1109/INDIN41052.2019.8972134.
[53] G. Schroeder *et al.*, “Visualising the digital twin using web services and augmented reality,” in *2016 IEEE 14th International Conference on Industrial Informatics (INDIN)*, Poitiers, France: IEEE, July 2016, pp. 522–527. doi: 10.1109/INDIN.2016.7819217.
[54] K. Dröder, P. Bobka, T. Germann, F. Gabriel, and F. Dietrich, “A Machine Learning-Enhanced Digital Twin Approach for Human-Robot-Collaboration,” *Procedia CIRP*, vol. 76, pp. 187–192, 2018, doi: 10.1016/j.procir.2018.02.010.

[55] M. Denk, S. Bickel, P. Steck, S. Götz, H. Völkl, and S. Wartzack, “Generating Digital Twins for Path-Planning of Autonomous Robots and Drones Using Constrained Homotopic Shrinking for 2D and 3D Environment Modeling,” *Appl. Sci.*, vol. 13, no. 1, p. 105, Dec. 2022, doi: 10.3390/app13010105.
[56] Z. Song, H. Shi, X. Bai, and G. Li, “Digital twin-assisted fault diagnosis system for robot joints with insufficient data,” *J. Field Robot.*, vol. 40, no. 2, pp. 258–271, Mar. 2023, doi: 10.1002/rob.22127.
[57] “Implementation of Trajectory Planning Algorithms for Track Serving Mobile Robot in ROS 2 Ecosystem,” *Teh. Vjesn. - Tech. Gaz.*, vol. 30, no. 4, Aug. 2023, doi: 10.17559/TV-20220823131848.
[58] A. Grazioso, A. Ugenti, R. Galati, G. Mantriota, and G. Reina, “Modeling and validation of a novel tracked robot *via* multibody dynamics,” *Robotica*, vol. 41, no. 10, pp. 3211–3232, Oct. 2023, doi: 10.1017/S0263574723000966.
[59] J. Xu *et al.*, “Path planning method for Camellia oleifera forest trenching operation based on human-robot collaboration,” *Comput. Electron. Agric.*, vol. 215, p. 108446, Dec. 2023, doi: 10.1016/j.compag.2023.108446.
[60] T. Zonta *et al.*, “Autonomous Snowblower Utilizing Internet of Things for Minimal Power Consumption,” in *2021 14th IEEE International Conference on Industry Applications (INDUSCON)*, São Paulo, Brazil: IEEE, Aug. 2021, pp. 686–693. doi: 10.1109/INDUSCON51756.2021.9529823.
[61] J. Selvanathan and H. Lang, “Design and development of an autonomous mobile patrol robot,” in *Progress in Canadian Mechanical Engineering. Volume 6*, Sherbrooke, Canada: Université de Sherbrooke. Faculté de génie, 2023. doi: 10.17118/11143/21107.
[62] X. Liu *et al.*, “Genetic Algorithm-Based Trajectory Optimization for Digital Twin Robots,” *Front. Bioeng. Biotechnol.*, vol. 9, p. 793782, Jan. 2022, doi: 10.3389/fbioe.2021.793782.
[63] Y. Ma, N. Xi, Y. Xue, S. Wang, Q. Wang, and Y. Gu, “Development of a UVC-based disinfection robot,” *Ind. Robot Int. J. Robot. Res. Appl.*, vol. 49, no. 5, pp. 913–923, June 2022, doi: 10.1108/IR-10-2021-0227.
[64] M. Narang *et al.*, “Fighting COVID: An Autonomous Indoor Cleaning Robot (AICR) Supported by Artificial Intelligence and Vision for Dynamic Air Disinfection,” in *2021 14th IEEE International Conference on Industry Applications (INDUSCON)*, São Paulo, Brazil: IEEE, Aug. 2021, pp. 1146–1153. doi: 10.1109/INDUSCON51756.2021.9529813.
[65] A. Adán, A. López-Rey, and A. Ramón, “Robot for thermal monitoring of buildings,” *Autom. Constr.*, vol. 154, p. 105009, Oct. 2023, doi: 10.1016/j.autcon.2023.105009.
[66] Q. Wang, W. Jiao, P. Wang, and Y. Zhang, “Digital Twin for Human-Robot Interactive Welding and Welder Behavior Analysis,” *IEEECAA J. Autom. Sin.*, vol. 8, no. 2, pp. 334–343, Feb. 2021, doi: 10.1109/JAS.2020.1003518.
[67] Q. Lv, R. Zhang, X. Sun, Y. Lu, and J. Bao, “A digital twin-driven human-robot collaborative assembly approach in the wake of COVID-19,” *J. Manuf. Syst.*, vol. 60, pp. 837–851, July 2021, doi: 10.1016/j.jmsy.2021.02.011.

[68] B. R. Galarza, P. Ayala, S. Manzano, and M. V. Garcia, “Virtual Reality Teleoperation System for Mobile Robot Manipulation,” *Robotics*, vol. 12, no. 6, p. 163, Nov. 2023, doi: 10.3390/robotics12060163.
[69] B. He, X. Cao, and Y. Hua, “Data fusion-based sustainable digital twin system of intelligent detection robotics,” *J. Clean. Prod.*, vol. 280, p. 124181, Jan. 2021, doi: 10.1016/j.jclepro.2020.124181.
[70] N. K. Chakshu, J. Carson, I. Sazonov, and P. Nithiarasu, “A semi-active human digital twin model for detecting severity of carotid stenoses from head vibration—A coupled computational mechanics and computer vision method,” *Int. J. Numer. Methods Biomed. Eng.*, vol. 35, no. 5, p. e3180, May 2019, doi: 10.1002/cnm.3180.
[71] B. R. Barricelli, E. Casiraghi, J. Gliozzo, A. Petrini, and S. Valtolina, “Human Digital Twin for Fitness Management,” *IEEE Access*, vol. 8, pp. 26637–26664, 2020, doi: 10.1109/ACCESS.2020.2971576.
[72] K. Amara, O. Kerdjidj, and N. Ramzan, “Emotion Recognition for Affective Human Digital Twin by Means of Virtual Reality Enabling Technologies,” *IEEE Access*, vol. 11, pp. 74216–74227, 2023, doi: 10.1109/ACCESS.2023.3285398.
[73] S. Davila-Gonzalez and S. Martin, “Human Digital Twin in Industry 5.0: A Holistic Approach to Worker Safety and Well-Being through Advanced AI and Emotional Analytics,” *Sensors*, vol. 24, no. 2, p. 655, Jan. 2024, doi: 10.3390/s24020655.
[74] A. E. Bondoc, M. Tayefeh, and A. Barari, “LIVE Digital Twin: Developing a Sensor Network to Monitor the Health of Belt Conveyor System,” *IFAC-Pap.*, vol. 55, no. 19, pp. 49–54, 2022, doi: 10.1016/j.ifacol.2022.09.182.
[75] A. E. Bondoc, M. Tayefeh, and A. Barari, “Employing LIVE Digital Twin in Prognostic and Health Management: Identifying Location of the Sensors,” *IFAC-Pap.*, vol. 55, no. 2, pp. 138–143, 2022, doi: 10.1016/j.ifacol.2022.04.183.
[76] A. E. Bondoc, M. Tayefeh, and A. Barari, “Learning phase in a LIVE Digital Twin for predictive maintenance,” *Auton. Intell. Syst.*, vol. 2, no. 1, p. 13, Dec. 2022, doi: 10.1007/s43684-022-00028-0.
[77] A. Ellman and P. Krus, “System Design Analytics with Low-Fidelity Models,” in *Advances in Computers and Information in Engineering Research, Volume 2*, ASME, 2021, pp. 359–385. doi: 10.1115/1.862025_ch12.
[78] T. Williams, X. Ribadeneira, S. Billington, and T. Kurfess, “ROLLING ELEMENT BEARING DIAGNOSTICS IN RUN-TO-FAILURE LIFETIME TESTING,” *Mech. Syst. Signal Process.*, vol. 15, no. 5, pp. 979–993, Sept. 2001, doi: 10.1006/mssp.2001.1418.
[79] M. A. Sheikh, S. T. Bakhsh, M. Irfan, N. B. M. Nor, and G. Nowakowski, “A Review to Diagnose Faults Related to Three-Phase Industrial Induction Motors,” *J. Fail. Anal. Prev.*, vol. 22, no. 4, pp. 1546–1557, Aug. 2022, doi: 10.1007/s11668-022-01445-2.
[80] R. Kumar *et al.*, “A State-of-the-Art Review on the Misalignment, Failure Modes and Its Detection Methods for Bearings,” *MAPAN*, vol. 38, no. 1, pp. 265–274, Mar. 2023, doi: 10.1007/s12647-022-00605-x.
[81] S. Al-Dossary, R. I. R. Hamzah, and D. Mba, “Observations of changes in acoustic emission waveform for varying seeded defect sizes in a rolling element

bearing," *Appl. Acoust.*, vol. 70, no. 1, pp. 58–81, Jan. 2009, doi: 10.1016/j.apacoust.2008.01.005.
[82] D. Petersen, C. Howard, N. Sawalhi, A. Moazen Ahmadi, and S. Singh, "Analysis of bearing stiffness variations, contact forces and vibrations in radially loaded double row rolling element bearings with raceway defects," *Mech. Syst. Signal Process.*, vol. 50–51, pp. 139–160, Jan. 2015, doi: 10.1016/j.ymssp.2014.04.014.
[83] V. Inturi, G. Sabareesh, K. Supradeepan, and P. Penumakala, "Integrated condition monitoring scheme for bearing fault diagnosis of a wind turbine gearbox," *J. Vib. Control*, vol. 25, no. 12, pp. 1852–1865, June 2019, doi: 10.1177/1077546319841495.
[84] C. Li, V. Sanchez, G. Zurita, M. Cerrada Lozada, and D. Cabrera, "Rolling element bearing defect detection using the generalized synchrosqueezing transform guided by time–frequency ridge enhancement," *ISA Trans.*, vol. 60, pp. 274–284, Jan. 2016, doi: 10.1016/j.isatra.2015.10.014.
[85] D. L. Logan, *A first course in finite element method*, Sixth edition. Australia: Cengage Learning, 2017.
[86] S. K. John, R. K. Mishra, K. Hari, H. P. Ramesha, and K. K. Ram, "Investigation of Bearing Failure in a Turbo Shaft Engine," *J. Fail. Anal. Prev.*, vol. 20, no. 1, pp. 34–39, Feb. 2020, doi: 10.1007/s11668-020-00812-1.
[87] R. Zhang, L. Guo, Z. Zong, H. Gao, M. Qian, and Z. Chen, "Dynamic modeling and analysis of rolling bearings with rolling element defect considering time-varying impact force," *J. Sound Vib.*, vol. 562, p. 117820, Oct. 2023, doi: 10.1016/j.jsv.2023.117820.
[88] S. M. Tayyab, S. Chatterton, and P. Pennacchi, "Intelligent Defect Diagnosis of Rolling Element Bearings under Variable Operating Conditions Using Convolutional Neural Network and Order Maps," *Sensors*, vol. 22, no. 5, p. 2026, Mar. 2022, doi: 10.3390/s22052026.
[89] SKF, *Quality standard for suppliers, edition 6.0*, 2023. [Online]. Available: https://cdn.skfmediahub.skf.com/api/public/094b318c22de5a74/pdf_preview_medium/094b318c22de5a74_pdf_preview_medium.pdf
[90] *ISO 9001:2015 Quality management systems - Requirements*, 2015. [Online]. Available: https://committee.iso.org/sites/tc176sc2/home/projects/published/iso-9001-2015.html#:~:text=ISO%209001%3A2015%20Quality%20management%20systems%20-%20Requirements%2C%20is,customer%20and%20applicable%20statutory%20and%20regulatory%20requirements%2C%20and
[91] K. L. Vahidova *et al.*, "Quality Management in Bearing Manufacturing," in *Proceedings of the International Symposium "Engineering and Earth Sciences: Applied and Fundamental Research" (ISEES 2018)*, Grozny. Russia: Atlantis Press, 2018. doi: 10.2991/isees-18.2018.55.
[92] FAG, "Condition monitoring using FAG products Technical Product Information." SCHAEFFLER GROUP INDUSTRIAL, 2007.
[93] *Rolling bearings. Measuring methods for vibration Radial ball bearings with cylindrical bore and outside surface*, 2nd ed. 2016.

[94] M. Wrzochal, “Comparative analysis of the structural solutions of bearing vibration test equipment used in quality control procedures,” *Int. J. Adv. Manuf. Technol.*, vol. 125, no. 9–10, pp. 4047–4063, Apr. 2023, doi: 10.1007/s00170-023-11029-5.
[95] A. M. Mahmoud, M. M. A. Lashin, F. Alrowais, and H. Karamti, “A Dual Soft-Computing Based on Genetic Algorithm and Fuzzy Logic Defect Recognition for Gearbox and Motors: Attempts Toward Optimal Performance,” *IEEE Access*, vol. 10, pp. 73956–73968, 2022, doi: 10.1109/ACCESS.2022.3188780.
[96] A. Barari and S. Mordo, “Effect of sampling strategy on uncertainty and precision of flatness inspection studied by dynamic minimum deviation zone evaluation,” *Int. J. Metrol. Qual. Eng.*, vol. 4, no. 1, pp. 3–8, 2013, doi: 10.1051/ijmqe/2012039.
[97] A. Barari, “Inspection of the machined surfaces using manufacturing data,” *J. Manuf. Syst.*, vol. 32, no. 1, pp. 107–113, Jan. 2013, doi: 10.1016/j.jmsy.2012.07.011.
[98] F. Pavese, A. Bošnjaković, S. Eichstädt, A. B. Forbes, and J. A. Sousa, *Advanced Mathematical and Computational Tools in Metrology and Testing XIII*, vol. 94. in Series on Advances in Mathematics for Applied Sciences, vol. 94. WORLD SCIENTIFIC, 2025. doi: 10.1142/14037.
[99] A. Barari, H. A. ElMaraghy, and G. K. Knopf, “Evaluation of Geometric Deviations in Sculptured Surfaces Using Probability Density Estimation,” in *Models for Computer Aided Tolerancing in Design and Manufacturing*, J. K. Davidson, Ed., Dordrecht: Springer Netherlands, 2007, pp. 135–146. doi: 10.1007/1-4020-5438-6_15.
[100] A. Barari, H. A. ElMaraghy, and W. H. ElMaraghy, “Design for Manufacturing of Sculptured Surfaces: A Computational Platform,” *J. Comput. Inf. Sci. Eng.*, vol. 9, no. 2, p. 021006, June 2009, doi: 10.1115/1.3130143.
[101] H. R. Najafabadi, T. G. Goto, T. C. Martins, A. Barari, and M. D. S. G. Tsuzuki, “Topology Optimization of Capacitive MEMS Accelerometers for Seismic Applications,” in *ICGG 2022 - Proceedings of the 20th International Conference on Geometry and Graphics*, vol. 146, L.-Y. Cheng, Ed., in Lecture Notes on Data Engineering and Communications Technologies, vol. 146. , Cham: Springer International Publishing, 2023, pp. 760–772. doi: 10.1007/978-3-031-13588-0_66.
[102] A. Alipanahi, M. Mahboubkhah, and A. Barari, “Cross-sensitivity control in a novel four-component milling dynamometer for simultaneous measurement of tri-axial forces and torque,” *Measurement*, vol. 191, p. 110788, Mar. 2022, doi: 10.1016/j.measurement.2022.110788.
[103] A. Barari, “Automotive body inspection uncertainty associated with computational processes,” *Int. J. Veh. Des.*, vol. 57, no. 2/3, p. 230, 2011, doi: 10.1504/IJVD.2011.044725.
[104] M. Aliakbari, M. Mahboubkhah, M. Sadaghian, A. Barari, and S. Akhbari, “Computer integrated work-space quality improvement of the C4 parallel robot CMM based on kinematic error model for using in intelligent measuring,” *Int. J. Comput. Integr. Manuf.*, vol. 35, no. 4–5, pp. 444–461, May 2022, doi: 10.1080/0951192X.2021.1992654.
[105] M. Mahboubkhah and A. Barari, “Design and development of a novel 4-DOF parallel kinematic coordinate measuring machine (CMM),” *Int. J. Comput. Integr.*

Manuf., vol. 32, no. 8, pp. 750–760, Aug. 2019, doi: 10.1080/0951192X.2019.1610576.
[106] E. Umaras, A. Barari, and M. S. G. Tsuzuki, "Tolerance analysis based on Monte Carlo simulation: a case of an automotive water pump design optimization," *J. Intell. Manuf.*, vol. 32, no. 7, pp. 1883–1897, Oct. 2021, doi: 10.1007/s10845-020-01695-7.
[107] T. Karacay and N. Akturk, "Experimental diagnostics of ball bearings using statistical and spectral methods," *Tribol. Int.*, vol. 42, no. 6, pp. 836–843, June 2009, doi: 10.1016/j.triboint.2008.11.003.
[108] H2W Technologies, "Non-Comm Moving Magnet Actuator." H2W Technologies, 2012. [Online]. Available: https://h2wtech.blob.core.windows.net/prod/pdf/2015-06-24-19-50-47.pdf
[109] "Linear Motion Calculator - H2W Technologies." [Online]. Available: https://www.h2wtech.com/page/linear-motion-calculator#Acceleration1
[110] A. W. Lees, S. Jana, D. J. Inman, and M. P. Cartmell, "The Control of Bearing Stiffness Using Shape Memory".
[111] P. R. Kuppens, M. A. Bessa, J. L. Herder, and J. B. Hopkins, "Monolithic binary stiffness building blocks for mechanical digital machines," *Extreme Mech. Lett.*, vol. 42, p. 101120, Jan. 2021, doi: 10.1016/j.eml.2020.101120.
[112] S. Groothuis, R. Carloni, and S. Stramigioli, "A Novel Variable Stiffness Mechanism Capable of an Infinite Stiffness Range and Unlimited Decoupled Output Motion," *Actuators*, vol. 3, no. 2, pp. 107–123, June 2014, doi: 10.3390/act3020107.
[113] G. Grioli *et al.*, "Variable stiffness actuators: The user's point of view," *Int. J. Robot. Res.*, vol. 34, no. 6, pp. 727–743, May 2015, doi: 10.1177/0278364914566515.
[114] H. Zhao, D. Han, L. Zhang, and S. Bi, "Design of a stiffness-adjustable compliant linear-motion mechanism," *Precis. Eng.*, vol. 48, pp. 305–314, Apr. 2017, doi: 10.1016/j.precisioneng.2016.12.013.
[115] X. Huang, Y. Li, S. W. Zhou, and Y. M. Xie, "Topology optimization of compliant mechanisms with desired structural stiffness," *Eng. Struct.*, vol. 79, pp. 13–21, Nov. 2014, doi: 10.1016/j.engstruct.2014.08.008.
[116] D. Bender and A. Barari, "Integrated Digital Design and Manufacturing for 3D Printing Technologies," *IFAC-Pap.*, vol. 52, no. 10, pp. 248–253, 2019, doi: 10.1016/j.ifacol.2019.10.031.
[117] "ANSYS Mechanical APDL Theory Reference." ANSYS, 2025. [Online]. Available: https://ansyshelp.ansys.com/public/account/secured?returnurl=/Views/Secured/corp/v251/en/wb_sim/ds_Home.html
[118] S. Tebby, A. Barari, and E. Esmailzadeh, "Development of Optimized Preliminary Vehicle Structural Model Using Simple Structural Beams-Frames (SSB) and Sub-Structural Analysis," *Comput.-Aided Des. Appl.*, vol. 11, no. 5, pp. 544–551, Sept. 2014, doi: 10.1080/16864360.2014.902685.